

**Chemical Engineering Journal**  
**Anaerobes supplemented with solely/dual nano-particles for bio-(H<sub>2</sub>&char) production from black liquor**  
--Manuscript Draft--

|                              |  |
|------------------------------|--|
| <b>Manuscript Number:</b>    | CEJ-D-20-08996   |
| <b>Article Type:</b>         | Research Paper   |
| <b>Section/Category:</b>     | Environmental Chemical Engineering   |
| <b>Keywords:</b>             | nutrient limitations; total reducing sugars; total phenolic compounds; enzymatic activities; extracellular polymeric substances  |
| <b>Corresponding Author:</b> | Ahmed Tawfik, Ph.D.<br>National Reaserach centre<br>Cairo, EGYPT   |
| <b>First Author:</b>         | Ahmed Tawfik, Ph.D.  |
| <b>Order of Authors:</b>     | Ahmed Tawfik, Ph.D.<br><br>Mohamed El-Qelish<br><br>Aida Galal<br><br>Zhong Yu<br><br>Mohamed A. Hassan<br><br>H. A. Salah<br><br>Mohamed S. Hasanin<br><br>Fangang Meng   |
| <b>Abstract:</b>             | Simultaneous bio- (H <sub>2</sub> &char) production and treatment of black liquor (BL) rich phenolic compounds was extensively investigated in batch anaerobic assays and pyrolysis experiments. The anaerobes were immobilized and loaded with 10 mg/gVS of the solely nanoparticles i.e. graphene (nG), graphene oxide (nGO), magnetite (nM), hydroxyapatite (nHap) and dual-nanoparticles of graphene/magnetite (nG/M) and graphene/hydroxyapatite (nG/Hap). Supplementation with solely nanoparticles enhanced the H <sub>2</sub> production and hydrogenase enzyme (HE) activities. However, the H <sub>2</sub> yield (HY) was maximized at a level of 115.9±12.2 ml /gCODs removed, 190.6 ±9.8 mL/g carbohydrate removed and 365.4 ±14.3 mL/g protein removed for nG/Hap due to an increase of enzymatic activities of the α-amylase, α-xylanase, CM-cellulase, polygalacturonase and protease by values of 52.5±1.6%, 26.4±0.9%, 32.7±1.4%, 0.7±0.04% and 29.2±1.5%, respectively. Moreover, the half maximal inhibitory concentration (IC50) was significantly (P≤0.5) reduced from 49.1±2.8 µg gallic acid equivalent/mL for BL to 13.1±2.8 µg gallic acid equivalent/mL for anaerobes supplemented with nG/Hap. Moreover, addition of nG/Hap reduced the lag phase from 72 hrs for control to 12.0 h, due to a high activity of HE (0.28 ± 0.004 mg M.B reduced/min). This indicates that the addition of nG/Hap rich of calcium ions accelerated the biodegradation activities and surprisingly the antioxidants activities - ABTS (Scavenging %) were significantly (P<0.5) increased from 31.9±2.9 to 89.9±0.28% due to the removal of total phenolic compounds (TPC) by a value of 45.9±1.2%. Microbial community analysis revealed that dual nanoparticles inhibited the competitors and promoted the cooperators for the hydrogen producers, i.e., Firmicutes. |
| <b>Suggested Reviewers:</b>  | Tsutomu OKUBO, ph-D<br>okubo@wangan.c.kisarazu.ac.jp<br><br>Pascal PEU, Prof.<br>pascal.peu@inrae.fr<br><br>Faizal Bux<br>faizalb@dut.ac.za  |
| <b>Opposed Reviewers:</b>    |  |

Dear Prof. Tejraj Aminabhavi,  
Co-Editor of Chemical Engineering Journal,

It is our pleasure to submit a manuscript entitled “*Anaerobes supplemented with solely/dual nano-particles for bio-(H<sub>2</sub>&char) production from black liquor*” for possible publication in CEJ journal.

Hydrogen fermentation of black liquor has recently got a great attention due to its high caloric value and as a clean biofuel. However, up-to- date the impact of immobilization of anaerobes on the solely and dual nanoparticles for bio-H<sub>2</sub> production from black liquor particularly on the enzymatic activities degrading proteins, carbohydrates, secretion of extracellular polymeric substances , ammonification, IC<sub>50</sub> and ABST was not carried out which extensively hereby addressed. Moreover, the immobilization of anaerobes on hydroxyapatite (nHap) and/or combined with Graphene is hereby investigated, where the nHap is rich with useful ions of phosphorus (P) and calcium (Ca) for micro-organisms. To our knowledge, there is no data in literature studying the impact of addition of nHap on the hydrogen producing bacteria from black liquor (BL). Therefore, the main objectives of this study are to investigate the impact of immobilization of anaerobes on the solely/dual nano-particles for mitigation the inhibition effect of phenolic compounds and promote the antioxidant activities, enzymatic activities for carbohydrates and proteins degradation, extracellular polymeric substances secretion and ammonification process during fermentation of black liquor. Meanwhile, the high throughput 16S rRNA sequencing was conducted to uncover bacterial community shift induced by the nanoparticles. The correlations between the community members were identified to further explore the effect of bacterial responses to nanoparticles on the overall hydrogen production of the anaerobes. Moreover, the bio-char production was assessed along with the cost-benefit analysis of the integrated process.

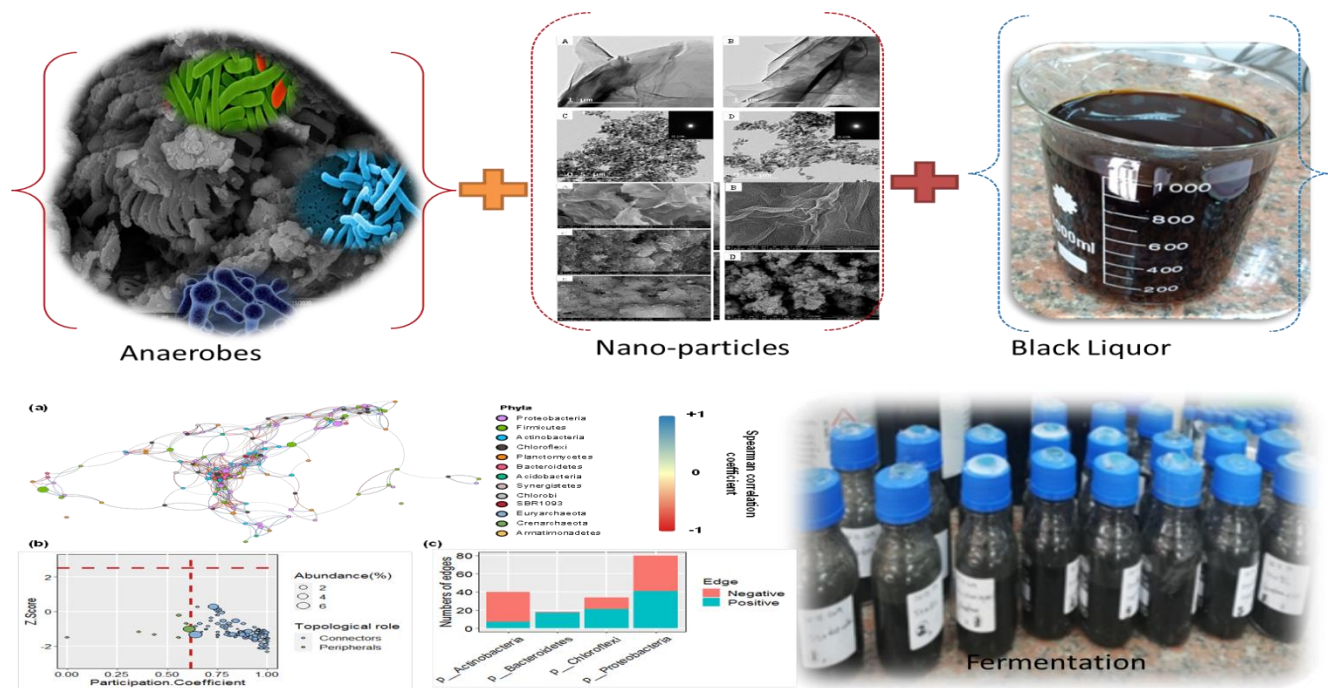
I hope you will consider our paper for publication in your journal,

Sincerely yours

Ahmed Tawfik

## List of reviewers

1. Tsutomu OKUBO, Ph.D.  
(Lecturer)  
Kisarazu National College of Technology  
Dept. of Civil & Environmental Engineering  
2-11-1 Kiyomidai-higashi, Kisarazu, Chiba 292-0041, JAPAN  
TEL & FAX: +81-438-30-4165  
E-mail: [okubo@wangan.c.kisarazu.ac.jp](mailto:okubo@wangan.c.kisarazu.ac.jp)
2. Prof. Shigeki Uemura  
Department of CIVIL and Environmental Engineering, Kisarazu national college of technology, Tel. +81-438-30-4152 Fax: +81-438-30-4152,  
[uemura@wangan.c.kisarazu.ac.jp](mailto:uemura@wangan.c.kisarazu.ac.jp)
3. Pascal PEU  
[pascal.peu@inrae.fr](mailto:pascal.peu@inrae.fr)  
**INRAE Bretagne-Normandie**  
**UR OPAALE**  
17 avenue de Cucillé  
35 044 Rennes Cedex  
+33 (0)2 23 48 21 45 (ligne directe)  
+33 (0)2 23 48 21 21 (standard)
4. Prof. Faizal Bux  
Director Institute for Water and Wastewater Technology  
Durban University of Technology  
P.O. Box 1334 Duran 4000  
Tel: +27313732597  
Fax:+27313732777  
[Email:faizalb@dut.ac.za](mailto>Email:faizalb@dut.ac.za)
5. Sheena Kumari Santosh  
[sheenas@dut.ac.za](mailto:sheenas@dut.ac.za)  
Institute for Water and Wastewater Technology,Durban University of Technology

**Graphical abstract**

## Highlights

- Immobilization of anaerobes on the solely and dual nano-particles improved HY
- nGraphene/hydroxyapatite reduces the inhibition effect of phenolic compounds
- Antioxidant activities was increased by supplementation of anaerobes with nano-particles
- Enzymatic activities were enhanced due to supplementation of dual nano-particles
- Ammonification and extracellular polymeric substances was maximized with nPS

1  
2  
3  
4 **Anaerobes supplemented with solely/dual nano-particles for bio-(H<sub>2</sub>&char) production**  
5  
6 **from black liquor**  
7  
8

9 **Mohamed El-Qelish<sup>1</sup>, Aida Galal<sup>1</sup>, Zhong Yu<sup>2</sup>, Mohamed A. Hassan<sup>3</sup>, H. A. Salah<sup>4</sup>,**  
10  
11 **Mohamed S. Hasarin<sup>5</sup>, Fangang Meng<sup>2</sup>, Ahmed Tawfik<sup>1</sup>♥**  
12  
13

14 <sup>1</sup> National Research Centre, Water Pollution Research Department 12622, Dokki, Cairo, Egypt  
15

16 <sup>2</sup>School of Environmental Science and Engineering, Sun Yat-sen University, Guangzhou  
17  
18 510006, PR China  
19  
20

21 <sup>3</sup>Agricultural Research Centre, Nanotechnology and Advanced Material Central Lab., Giza,  
22  
23 Egypt  
24  
25

26 <sup>4</sup>National Research Centre, Molecular Biology Department, 12622, Dokki, Cairo, Egypt  
27  
28

29 <sup>5</sup>National Research Centre, Cellulose and Paper Department, 12622, Dokki, Cairo, Egypt  
30  
31  
32

33 **Abstract**  
34  
35

37 Simultaneous bio- (H<sub>2</sub>&char) production and treatment of black liquor (BL) rich phenolic  
38 compounds was extensively investigated in batch anaerobic assays and pyrolysis experiments.  
39 The anaerobes were immobilized and loaded with 10 mg/gVS of the solely nanoparticles i.e.  
40 graphene (nG), graphene oxide (nGO), magnetite (nM), hydroxyapatite (nHap) and dual-  
41 nanoparticles of graphene/magnetite (nG/M) and graphene/hydroxyapatite (nG/Hap).  
42 Supplementation with solely nanoparticles enhanced the H<sub>2</sub> production and hydrogenase enzyme  
43 (HE) activities. However, the H<sub>2</sub> yield (HY) was maximized at a level of 115.9±12.2 ml /gCODs  
44 removed, 190.6 ±9.8 mL/g carbohydrate removed and 365.4 ±14.3 mL/g protein removed for nG/Hap due  
45 to an increase of enzymatic activities of the α-amylase, α-xylanase, CM-cellulase,  
46  
47  
48  
49  
50  
51  
52  
53  
54  
55  
56  
57  
58  
59  
60  
61  
62  
63  
64  
65

---

• Corresponding author: [prof.ahmed.tawfik@gmail.com](mailto:prof.ahmed.tawfik@gmail.com) (A.Tawfik)

polygalacturonase and protease by values of  $52.5\pm1.6\%$ ,  $26.4\pm0.9\%$ ,  $32.7\pm1.4\%$ ,  $0.7\pm0.04\%$  and  $29.2\pm1.5\%$ , respectively. Moreover, the half maximal inhibitory concentration ( $IC_{50}$ ) was significantly ( $P\leq0.5$ ) reduced from  $49.1\pm2.8$   $\mu$ g gallic acid equivalent/mL for BL to  $13.1\pm2.8$   $\mu$ g gallic acid equivalent/mL for anaerobes supplemented with nG/Hap. Moreover, addition of nG/Hap reduced the lag phase from 72 hrs for control to 12.0 h, due to a high activity of HE ( $0.28 \pm 0.004$  mg M.B reduced/min). This indicates that the addition of nG/Hap rich of calcium ions accelerated the biodegradation activities and surprisingly the antioxidants activities -ABTS (Scavenging %) were significantly ( $P<0.5$ ) increased from  $31.9\pm2.9$  to  $89.9\pm0.28\%$  due to the removal of total phenolic compounds (TPC) by a value of  $45.9\pm1.2\%$ . Microbial community analysis revealed that dual nanoparticles inhibited the competitors and promoted the cooperators for the hydrogen producers, i.e., *Firmicutes*. The digestate resulted from fermentation of sludge, BL and nG/Hap were further pyrolyzed for bio-char production at temperature of  $550$  °C for 1.0 h. The bio-char exhibited a specific surface area of  $2.4 \pm 0.95$   $m^2/g$ , density of  $1.63 \pm 0.18$   $g/cm^3$ , pore volume of  $0.2 \pm 0.06$   $cm^3/g$  and yield ( $33\pm5.2\%$ ). The maximum overall profit from both  $H_2$  and bio-char was  $3000$  \$/ $m^3$ .

**Keywords:** nutrient limitations; total reducing sugars; total phenolic compounds; enzymatic activities; extracellular polymeric substances

## 1. Introduction

Agriculture wastes such as rice straw (RS) and sugar cane bagasse (SCB) are abundant and cause severe environmental problems due to a lack of proper management and financial support in developing countries. The RS and SCB are partially utilized for ethanol production and paper making industry. However, the chemical pulping process of RS and SCB produces considerable

1  
2  
3  
4 quantities of black liquor (BL) rich of phenolic compounds and non-biodegradable organics.  
5  
6 Uncontrolled discharge and /or dumping of BL onto the environment cause severe health  
7 problems and water pollution. Fortunately, the BL is rich of carbohydrates, sugars, proteins and  
8 phosphorous, which can be easily utilized by micro-organisms to produce valuable by-products.  
9 Nevertheless, physio-chemical treatment processes have been previously employed for treatment  
10 of BL i.e. dissolved air flotation [1], coagulation and precipitation [2], adsorption [3],  
11 photocatalytic oxidation [4], fenton and photo-fenton reactions [5], membrane filtration [6] and  
12 ozonation [7]. Those technologies are consuming energy, chemicals and produce high volumes  
13 of sludge which needs further treatment processes. Aerobic treatment processes have been also  
14 attempted for treatment of BL and/or pulp –paper mill industry [8]. The activated sludge process  
15 suffered and failed in the treatment of such wastewater due to their toxicity and aerobic bacteria  
16 are very sensitive to high content of phenolic compounds [9]. Moreover, filamentous bacteria are  
17 dominated in the activated sludge units treating pulp and paper mill wastewater causing sludge  
18 bulking and poor removal efficiency of pollutants [10]. However, integration of anaerobic –  
19 aerobic process was successfully employed and minimized the cost and the sludge production for  
20 the treatment of black liquor (BL) [11]. To our knowledge the hydrogen fermentative of BL is  
21 scarce in literature.

22

23

24

25

26

27

28

29

30

31

32

33

34

35

36

37

38

39

40

41

42

43

44

45

46

47

48 Hydrogen fermentation of BL has recently got a great attention due to its high caloric value and  
49 as a clean biofuel. The hydrogen is an eco-friendly energy candidate and could be utilized for  
50 electricity generation using fuel cell. In addition, it could be used as a feedstock for many  
51 industries such as bio-fertilizers production by combination with the nitrogen from air.  
52  
53 Hydrogen could substitute fossil fuels, minimizing the CO<sub>2</sub> emission. Hydrogen production from  
54  
55  
56  
57  
58  
59  
60  
61  
62  
63  
64  
65

BL has been attempted by electrolysis [12,13], supercritical water gasification & syngas chemical looping [14] and gasification [15]. Hydrogen fermentative process is still the promising approach and eco-friendly technology where the cost and excess sludge is kept quite low. Anaerobic technology for H<sub>2</sub> production from BL is very competitive technology particularly for the countries suffering from a lack of financial support and fossil fuels. The H<sub>2</sub> production (HP) still does not take that great attention from the decision makers in the developing countries due to the relatively low production and yield of 55.4 ml/g-COD removed [16]. Moreover, it is hardly to find a literature concerning H<sub>2</sub> production from alkaline and nutrients deficient BL using anaerobes which are comprehensively addressed in this research work.

Several attempts have been tried to increase the H<sub>2</sub> production (HP) and yield (HY) from low value substrates, i.e. HP from industrial wastewater containing mono-ethylene glycol was significantly increased by 41, 30, and 29%, for anaerobes individually supplemented with  $\alpha$ -Fe<sub>2</sub>O<sub>3</sub> (200 mg/l), NiO (20 mg/l), and ZnO NPs (10 mg/l), respectively[17]. Further improvement of HY was occurred with the immobilization of anaerobes on dual and multi-NPs due to the increase of *Clostridiales* (belonging to family *Clostridiaceae*; > 83%) in the reaction medium [18]. Addition of hematite nanoparticles to the anaerobes fed with sucrose wastewater increased the hydrogen production rate (HPR) from 3.87 to 5.9 l/L.d [19]. Mixed culture bacteria supplemented with 100 mg/l magnetite/graphene oxide (MGO) and fed with gelatinous wastewater industry promoted HY up to 112.4  $\pm$  10.5 ml H<sub>2</sub>/gCOD removed and provided degradation efficiency of 80.8  $\pm$  7.6% for carbohydrates, 34.4  $\pm$  2.3% for proteins and 31.4  $\pm$  2.2% for lipids due to the enhancement of *Proteobacteria*, *Firmicutes*, *Clostridia* and *Bacilli*

1  
2  
3  
4     activities [20]. NiCo<sub>2</sub>O<sub>4</sub>-graphene nano-composites decorated with NF exhibited HPR of 0.14 ±  
5     0.003 l/l .d which was 3.2 times higher than control samples [21].  
6  
7  
8  
9  
10  
11  
12  
13  
14  
15  
16  
17  
18  
19  
20  
21  
22  
23  
24  
25  
26  
27  
28  
29  
30  
31  
32  
33  
34  
35  
36  
37  
38  
39  
40  
41  
42  
43  
44  
45  
46  
47  
48  
49  
50  
51  
52  
53  
54  
55  
56  
57  
58  
59  
60  
61  
62  
63  
64  
65

Up-to- date the impact of immobilization of anaerobes on the solely and dual nanoparticles for bio-H<sub>2</sub> production from BL particularly on the enzymatic activities degrading proteins, carbohydrates, secretion of extracellular polymeric substances (EPS), ammonification, IC<sub>50</sub> and ABST was not carried which extensively hereby addressed. Moreover, the immobilization of anaerobes on hydroxyapatite (nHap) and/or combined with graphene is hereby investigated, where the nHap is rich with useful ions of phosphorus (P) and calcium (Ca) for micro-organisms. To our knowledge, the nG/Hap was only studied for the removal of methylene blue (MB) dye from wastewater [22], NiFe<sub>2</sub>O<sub>4</sub>/hydroxyapatite/graphene for removal of cadmium (Cd<sup>2+</sup>) from wastewater [23], biomedical applications [24], capture of strontium [25], photocatalyst and adsorption of Pb(II) ions [26,27] and there is no data in literature studying the impact of addition of nHap on the hydrogen producing bacteria from BL.

Therefore, the main objectives of this study are to investigate the impact of immobilization of anaerobes on the solely/dual nano-particles for mitigation the inhibition effect of phenolic compounds and promote the antioxidant activities, enzymatic activities for carbohydrates and proteins degradation, extracellular polymeric substances secretion and ammonification process during fermentation of black liquor (BL). Meanwhile, the high throughput 16S rRNA sequencing was conducted to uncover bacterial community shift induced by the nanoparticles. The correlations between the community members were identified to further explore the effect of bacterial responses to nanoparticles on the overall hydrogen production of the anaerobes.

Moreover, the bio-char production was assessed along with the cost-benefit analysis of the integrated process.

## 2. Materials and Methods

### 2.1. Black liquor (BL) composition

The black liquor (BL) was harvested from paper making industry facility. The rice straw (RS) is the main source for manufacturing company which is abundant in Egypt. The RS was alkali pretreated by sodium hydroxide (1.75% w/v) at a temperature of 180 °C and pressure of 1.5 bars for 2 hrs. BL was brownish in color with a pH value exceeding 12.75 which was neutralized to be 7.5 by phosphoric acid (77% conc.) to enrich the substrate with nutrients for bio-degradation processes. The BL contained suspended fibers in the bulk liquid and their characteristics are presented in **Table 1a**. The BL was mainly in a soluble form where the soluble COD (CODs) represented 98% of the total COD (CODt) and the particulate fraction was quite low (2.0%). The volatile solids to total solids (VS/TS) ratio were 0.5 due to the use of NaOH and H<sub>3</sub>PO<sub>4</sub> for pre-treatment and neutralization of raw materials, respectively. The COD: N: P ratio of the BL was 12.3: 1: 3.2 and C/P ratio was 3.85. The total phenolic compounds (TPC) in the BL amounted to 1718±12.4 mg/L resulting a half maximal inhibitory concentration (IC<sub>50</sub>) of 48.4±0.3 µg Gallic acid equivalent/ mL. Scanning electron microscope (SEM) and energy dispersive X-Ray (EDX) analysis were carried out for the BL (**Fig.1a and Table 1b**). The SEM image clearly showed the morphology of the dry crystals of the BL and the presence of fibers in the samples (**Fig. 1a**). Those fibers could be the remaining portions of lignin, cellulose and hemicellulose after alkali pre-treatment process. The oxygen and carbon represented 65% of the total weight of the elements (**Table 1b**). Sodium (Na) element percentage was quite high (26.59%) due to the alkali-

1  
2  
3  
4 pretreatment of rice straw. As expected the silica content was 5.2% and potassium (K) was  
5  
6 2.32%.  
7  
8  
9  
10  
11  
12  
13

14 *2.2.Mixed culture anaerobes*  
15  
16  
17  
18

19 The anaerobes were collected from a full scale anaerobic digester located in Al-Gabal Al-Asfer,  
20 Cairo, Egypt. The sludge was dark black in color. The settleability of the inoculum sludge was  
21 quite high and amounted to 30 ml/gTS. The characteristics of the inoculum sludge are presented  
22 in **Table 1a**. The TS and VS contents were  $132.04 \pm 0.34$  and  $72.75 \pm 0.35$  g/l. The VS/TS ratio of  
23 the sludge was 0.55. The anaerobes were daily supplemented with BL for acclimatization period  
24 of 30 days. The CODs was quite low and represents 5% of the CODt. The CODp/CODt ratio  
25 was 0.95. The seed sludge was free from iso-butyrate (iso-HBu), propionate (HPr), formate  
26 (HFo) and acetate (HAc).  $\alpha$ -amylase-,  $\alpha$ - xylanase (used breach xylan), CM-cellulase (CM-  
27 cellulose) was  $9.0 \pm 0.4$ ,  $400 \pm 7.8$ ,  $15 \pm 1.2$  and  $4.1 \pm 0.7$  U/100 mL, respectively. SEM and EDX  
28 analysis were carried out for the inoculum sludge after adaptation process (**Fig. 1a**). The  
29 morphology of sludge is compacted and flocculent free from granulation. The EDX analysis  
30 showed the sludge is rich of carbon (44.39%) and oxygen (30.96%). The sludge contained a  
31 percent of 5.12% for nitrogen, 3.19% for phosphorous, 2.36% for sulfur and 4.1% for calcium.  
32  
33  
34  
35  
36  
37  
38  
39  
40  
41  
42  
43  
44  
45  
46  
47  
48  
49  
50  
51  
52

53 *2.3.Preparation of solely and dual nanoparticles*  
54  
55  
56  
57  
58  
59  
60  
61  
62  
63  
64  
65

1  
2  
3  
4 Analytical grade chemicals were purchased from Sigma Aldrich for preparation of graphene  
5 oxide (nGO), graphene (nG), Magnetite (nM), graphene/magnetite (nG/M), hydroxyapatite  
6 (nHap) and graphene/hydroxyapatite (nG/Hap) at a nano-scale. A modified Hummers method  
7 was used to synthesize nGO in nano-scale from graphite powder as carbon precursor as  
8 previously described earlier by Chen [28].  
9  
10  
11  
12  
13  
14

15  
16  
17  
18 Graphene nano-sheets were prepared using the solvothermal method using ethylene glycol and  
19 graphene oxide (GO). 1.5 g of the previously prepared nGO was suspended in ethylene glycol  
20 (240 ml) and strongly sonicated for 15 min. in ultrasonic waves equipped with probe. The  
21 suspension was carefully transferred in a stainless steel Teflon lined autoclave and incubated for  
22 a period of 24 h., at a temperature of 180 °C. The black solution was produced, immediately  
23 washed and filtrated several times by deionized H<sub>2</sub>O and Et-OH. The mixture was allowed to be  
24 dried overnight at a temperature of 70 °C.  
25  
26  
27  
28  
29  
30  
31  
32  
33  
34

35  
36  
37 Magnetite nanoparticles (nM) were prepared under continuous nitrogen gas flow. 0.82725 g of  
38 ferric chloride (FeCl<sub>3</sub>, M.Wt 162.2) and 1.0 g of ammonium ferrous sulfate  
39 (NH<sub>4</sub>)<sub>2</sub>Fe(SO<sub>4</sub>)<sub>2</sub>.6H<sub>2</sub>O, was added to a 50 ml solution of NaOH (3.0 M) and continuously stirred  
40 to complete solubilization of the iron salts in the reaction medium. A brown color is formed at  
41 pH value of 2-3 which was further increased up to 10.0 using NaOH solution (3.0 M) resulting a  
42 black color precipitate. The latter was carefully filtrated, washed several times with deionized  
43 H<sub>2</sub>O and dried at a temperature of 35 °C for 24h.  
44  
45  
46  
47  
48  
49  
50  
51  
52  
53  
54  
55  
56  
57  
58  
59  
60  
61  
62  
63  
64  
65

Graphene/magnetite (nG/M) was prepared and synthesized using Solvothermal method where 5.0 g of sodium acetate was added to an ultrasonicated graphene oxide solution (0.5 g) and mixed in 80 ml ethylene glycol. 0.42 g FeCl<sub>3</sub> was added to the previous solution under continuous flow of nitrogen gas. This mixture was carefully transferred into an autoclave Teflon-lined stainless steel and heated at a temperature of 200 °C for a period of 10 h. The obtained black powder was washed several times with Et-OH and deionized H<sub>2</sub>O, then dried in a vacuum oven at a temperature of 60 °C.

Hydroxyapatite nanoparticles (nHap) was prepared based on a stoichiometric molar ratio of 1.67 (Ca/P), by addition of 0.8 mol. (Ca (NO<sub>3</sub>)<sub>2</sub>.4H<sub>2</sub>O and 0.479 mol H<sub>3</sub>PO<sub>4</sub> in a sol-gel method. Ammonia solution was used to adjust the pH value at a level of 10.0±0.05. Ca (NO<sub>3</sub>)<sub>2</sub>.4H<sub>2</sub>O solution was vigorously stirred at a temperature of 25 °C and phosphoric acid was drop-wisely added at a flow rate of 3 ml/min. The suspension was left under vigorous stirring for a time of 16 h., and after 24 h., of aging, the precipitate was rinsed with deionized H<sub>2</sub>O and dried at a temperature of 100 °C under vacuum.

Graphene/ hydroxyapatite (G/nHap) was prepared by hydrothermal treatment of the mixture of 600 mg of nGO, 8 mM of CaCl<sub>2</sub>, 4.8 mM (NH<sub>4</sub>)<sub>2</sub>(HPO<sub>4</sub>) and the pH value of 10.0 was adjusted using ammonium hydroxide. Afterwards, the mixture was heated in a stainless steel Teflon lined autoclave at a temperature of 180 °C for a period of 24 h. The composite was regularly separated using centrifugation, washed by distilled H<sub>2</sub>O & Et-OH ethanol and dried overnight at a temperature of 70 °C.

1  
2  
3  
4     *2.4. Experimental set-up*  
5  
6  
7  
8  
9  
10  
11  
12  
13  
14  
15  
16  
17  
18  
19  
20  
21  
22  
23  
24  
25  
26  
27  
28  
29  
30  
31  
32  
33  
34  
35  
36  
37  
38  
39  
40  
41  
42  
43  
44  
45  
46  
47  
48  
49  
50  
51  
52  
53  
54  
55  
56  
57  
58  
59  
60  
61  
62  
63  
64  
65

Anaerobic batch assays experiments were carried out in triplicate for a period of 14.0 days (350 hrs) (**Fig. 1b**). The serum bottles with a capacity of 300 ml were used for the experiments. The 1<sup>st</sup> bottles set was supplied with 100 ml sludge (S) (mixed culture anaerobes) and 150 mL dist. water. Those bottles were used as a control to assess the gas production from the sludge. The 2<sup>nd</sup> bottles set were supplemented with 100 mL sludge (S) (7.2 gVS/100mL) and 150 mL black liquor (BL) (3.3 g CODt/150 mL) resulting food to microorganism (F/M) ratio of 0.46 gCODt/gVS in the reaction medium. The main reaction bottles sets were inoculated with the following components i.e. 100 mL (S)+ 150 mL (BL) + 10 mg/gVS (nG); 100 mL (S)+ 150 mL (BL) + 10 mg/gVS (nGO); 100 mL (S)+ 150 mL (BL) + 10 mg/gVS (nM); 100 mL (S)+ 150 mL (BL) + 10 mg/gVS (nG/M), 100 mL (S)+ 150 mL (BL) + 10 mg/gVS (nHap) and 100 mL (S)+ 150 mL (BL) + 10 mg/gVS (nG/Hap). pH value of all bottles set were adjusted at a level of 7.5 using phosphoric acid to be utilized as a source of nutrient and suitable for growth of anaerobes. The batches had a head space of 50 mL to allow the gas production and the bottles were flushed for 3 minutes using nitrogen gas to create perfect anaerobic conditions in the reaction medium. The bottles set was incubated at a temperature of 35 ± 0.2 °C. The volumetric gas production was daily measured along fermentation time of 350 hrs using a syringe avoiding interference with others. The biogas composition was daily measured and the hydrogen potential (P- mL), maximum hydrogen production rate ( $R_{max}$ - mL /h) was simulated based on Gomportze equation model (**Eq. 1**),

$$H(t) = P * \exp \left\{ - \exp \left( \frac{R_{max} * e}{P} (\lambda - t) + 1 \right) \right\} \quad Eq. 1$$

Where  $H$ : is the cumulative  $H_2$  production (mL),  $t$ : is the fermentation time (h) and  $\lambda$ : is the lag phase duration (h)

### *2.5. Pyrolysis process for bio-char production and net energy calculations*

This experiment was conducted to fully utilize the black liquor (BL) providing a zero waste technology via bio-(H<sub>2</sub> & char) production. Duplicate samples (50 ml) of the digestate resulted from anaerobic digestion of sludge (S), black liquor (BL) and nG/Hap (10 mg/gVSS) was placed in a porcelain dish and burnet at temperature of 550 °C for a period of 1.0 h. The bio-char amounted to 330±10.9 g/L digestate which represented to 33%. The required energy for conversion of the digestate into bio-char followed the auger-based pyrolysis system. Two steps are basically carried out for pyrolysis processes i.e. the reduction moister and digestate drying at an oxygen-free environment at 550 °C. Vapors released from the pyrolysis step are mainly recycled to maximize the drying step as well as operating the pyrolyzer [29]. Characterization and analysis of the bio-char were carried out for further reuse in agricultural purposes. Economic and cost benefit analysis of the combined process (fermentation/pyrolysis) was assessed. The energy consumption for anaerobic digestion process is mainly utilized for mixing and heating the digester. The following equation (**Eq. 2**) was used to calculate the energy consumption for heating the reactor up to 35 °C.

$$E_H = C_p * M * dT / x \quad Eq. 2$$

Where,  $E_H$ : is the energy required for heating the reactor (kJ/l feedstock);  $C_p$ : is the specific heat constant ( $C_p$  of the water = 4.186 kJ/kg.K);  $M$ : is the weight of the sludge inside the batch reactor (kg),  $x$ : is the influent total solids and  $dT$ : is the difference between the initial (20 °C) and operational temperature (35 °C) [30]. The energy consumed for mixing  $E_m$  was calculated based

on the horse power of the mixer (0.05 HP) and operational time. Hydrogen energy  $E_{H_2}$  (kJ/Lfeedstock) was estimated from **Eq. 3**,

$$E_{H_2} = G * \rho_{H_2} * LHV_{H_2}/x \quad Eq. 3$$

Where,  $G$  :is the volume of hydrogen (L);  $\rho_{H_2}$  : is the density of hydrogen gas ( $8.9 \times 10^{-5}$  kg/L); and LHV is the lower heating value of hydrogen (120,000 kJ/kg) [30].

$$Net_{energy}(Kj/l)substrate = E_{H_2} - E_H - E_M \quad Eq. 4$$

The net energy was calculated from **Eq.4** where hydrogen energy ( $E_{H_2}$ ), was subtracted from  $E_H$  and  $E_M$ . The electrical energy cost utilized for bio-char production was estimated by Huang et al., [31] to be 43 \$/feedstock for a small scale auger-based pyrolysis system.

### 2.6. Analytical methods

The black liquor (BL), sludge (S) and nanoparticles ( $N_p$ ) were analyzed. The pH value was measured by a device of JENWAY 3510. COD<sub>t</sub>, COD<sub>s</sub>, COD<sub>p</sub>, total solids (TS), volatile solids (VS), total phosphorous (TP), TKJ-N and NH<sub>4</sub>-N were determined based on APHA [32]. COD<sub>s</sub> was filtered using membrane filter (0.45 μm) and the COD<sub>p</sub> was calculated by the difference between COD<sub>t</sub> and filtered COD. Volatile fatty acids (VFAs) in terms of formate (HFo), propionate (HPr), iso-butyrate (HBu), acetate (HAc), valerate (HVa) were determined by High Performance Liquid Chromatography (HPLC). Scanning electron microscopy (SEM) and energy dispersive X-Ray (EDX) was used to observe the morphology of the sludge and elemental

analysis content. Transmission electron microscope TEM, Model JEM-2010, Japan, was used to investigate particle size and morphology. Fourier-transform infrared spectroscopy (FTIR) analysis was used to detect the presence of the main organic groups that constitute the BL, sludge and bio-char. FTIR analysis was carried out in the range of 450 to 4000 cm<sup>-1</sup> using a Fourier Transform infrared spectrophotometer (JASCO 6100 spectrometer, Japan). X-Ray Diffraction (Schimadzu XRD 7000, Japan) and a Thermo Scientific, Trace GC Ultra / ISQ Single Quadrupole MS, TG-5MS fused silica capillary column (30m, 0.251mm, 0.1 mm film thickness) was used for characterization of the BL and S samples. Enzymatic assays of microbial carbohydrate-cleaving enzymes in terms of polygalacturonase,  $\alpha$ -xylanase, CM-cellulase and  $\alpha$ -amylase (EC3.2.1.1) activities were measured by determination of the liberated reducing end products using galacturonic acid, xylose, glucose and maltose, respectively as standards [33]. One unit of enzyme activity was defined as the amount of enzyme which liberated 1  $\mu$ mol of reducing sugar/h under standard assay conditions. The total phenolic content of the samples was measured by the method described earlier by Velioglu et al. [34]. The results are expressed as mg gallic acid equivalent (GAE)/ ml according to a gallic acid standard curve. The antioxidant activity of the samples was determined by (2, 2-azino-bis (3-ethylbenzo-thiazoline-6-sulfonic acid) (ABTS) based on the method of Re et al., [35] and Eq. 5. Carbohydrates were determined by the method of Dubois et al. [36]. Glucose served as the calibration standard for total carbohydrate determination. The reduction method of methylene blue was used for measurement of hydrogenase enzyme activity[37]. Protein content was determined as described by Emami Bistgani et al., [38] using bovine serum albumin as standard.

$$ABTS \text{ scavenging } (\%) = \left\{ \frac{O.D_{control} - O.D_{sample}}{O.D_{control}} \right\} \times 100 \quad Eq. 5$$

## 2.7. Microbial analysis community

1  
2  
3  
4  
5  
6     2.7.1. DNA extraction  
7  
8  
9  
10

11     The batch samples supplemented with nG/Hap, nG/M, nM and nHap (denoted as N1, N2, N3  
12     and N4, respectively) were aliquoted after fermentation and stored at -20 °C for DNA analysis.  
13  
14

15     Cells were pelleted by centrifugation (6000g, 10 min) before DNA extraction. The Macherey  
16     Nagel NucleoSpin Soil kit was used for DNA extraction from 300 mg of pellet according to the  
17     manufacturer's instructions. The extracted DNA was carefully eluted in 100 µL of sterile water  
18     and stored at temperature of -20°C for further analysis. Spectrophotometry (ND-1000, Nanodrop  
19     Tech.) was thoroughly used to check the concentration and purity of DNA and subsequently,  
20     DNA quality was determined on 0.7% agarose gel in Tris Borate EDTA (TBE) 1X Buffer.  
21  
22  
23  
24  
25  
26  
27  
28  
29  
30  
31  
32  
33     2.7.2. Quantitative PCR (qPCR)  
34  
35  
36  
37  
38     The archaeal and bacterial communities of each sample were quantified using qPCR techniques  
39     targeting the 16S rRNA gene. All qPCR amplifications were determined according to the  
40     supplier's instructions using CFX thermal cycler (BioRad). The mixtures of 25 µL contained  
41     12.5 µL of iQ Sybr Green supermix 2X (BioRad), 1.5 µL (10 µM) of each primer set 1055F (5'-  
42     ATGGCTGTCGTAGCT-3') and 1392R (5'-ACGGGCGGTGTGTAC-3') for bacteria or 0.5  
43     µL (10 µM) of ARC787F (5'-ATTAGATACCSBGTAGTCC-3') and ARC1059R (5'-  
44     GCCATGCACCWCCTCT-3') for archaea, 2 µL of template DNA, and the remaining portion as  
45     sterile water. The amplification reaction process for bacterial communities was: initial  
46     denaturation at temperature of 94 °C for 10 min followed by 45 cycles of 95 °C for 30 s, 60 °C  
47  
48  
49  
50  
51  
52  
53  
54  
55  
56  
57  
58  
59  
60  
61  
62  
63  
64  
65

for 50 s, and 72 °C for 30s. The amplification reaction for Archaea was: initial denaturation at a temperature of 95 °C for 15 min, followed by 45 cycles of 95 °C for 15 s, 50 °C for 20 s, and 72°C for 1 min. Finally, a melting curve analysis was assessed to check the specificity of amplification and primer dimers formation. Standard curve was drawn up by 10-fold dilution of an initial solution of bacterial community or archaeal PCR product with a known concentration. All samples and standards was carried out in triplicates and the gene copy numbers were estimated by comparison with DNA standards of known concentrations.

#### 2.7.3. Community analysis using Single Strand Conformation Polymorphism (SSCP)

Bacterial community analysis was carried out by PCR-SSCP amplification as earlier described by Delbès et al. [39]. Bacterial primers W49 (5'-ACGGTCCAGACTCCTACGGG-3') and 5'FAM W34 (5'-FAM-TTACCGC GGCTGCTGGCAC-3') were efficiently used to target 200 bp of the 16S rRNA gene V3 region. Each PCR mixture contains 2.0 µL of 10X *Pfu* turbo DNA polymerase buffer (Agilent Technologies), 200 µM of each *dNTP*, 0.25 µM of each primer, 0.2 µL of *Pfu* turbo DNA polymerase (Agilent Technologies). The PCR reaction was carried out as follows: initial denaturation at temperature of 94 °C for 2 min, followed by 25 cycles at 94 °C for 30 s, 61°C for 30 s, 72 °C for 30s, with final step at 72°C for 10 min. Amplifications were assessed with a T100 thermal cycler (BioRad). One µL of diluted PCR product was mixed with 18.8 µL of formamide and 0.2 µL of internal standard 400HD Genescan ROX (Applied Biosystems). Samples were denatured at a temperature of 95 °C for 5 min and immediately cooled in the ice. Capillary-Electrophoresis-SSCP (CE-SSCP) was performed on ABI 310 Genetic Analyzer [39].

1  
2  
3  
4     2.7.4.OTU assignments and statistical analysis  
5  
6  
7  
8  
9  
10

The extracted DNA was further used for the amplification of the bacterial and archaeal hypervariable region V4–V5 of the 16S rRNA gene with primers 515F (5'-GTGYCAGCMGCCGCGTA-3') and 928R (5'-CCCGYCAATTCTTTRAGT-3') as previously described by Poirier et al. [40]. The Quantitative Insights into Microbial Ecology (QIIME) software was used to analyze of the sequences [41]. In particular, quality filtered sequence data was exported as FastQ file (15,000 to 90,000 reads for each sample). The quality of reads were carefully checked by three amplicon read processing pipelines i.e. MOTHUR v.1.25.0 [42], QIIME 1.8.0 [41], and USEARCH v5.2.136 [43]. Low quality score (<20) and/or sequences shorter than 180 bp were removed. Chimeric sequences were totally removed and sequences were clustered into Operational Taxonomic Units (OTUs) with 97% sequence similarity using quality filter (USEARCH) (<http://www.drive5.com/usearch/>) reference set[44]. A representative sequence for each OTU was selected based on the longest sequence in each OTU and assigned to the corresponding taxa using the Ribosomal Database Project (RDP) classifier. Furthermore, the Chao1, ACE, Simpson, and Shannon indices were calculated based on the rarefied OTU table using the package ‘vegan’ in R [45]. The relative abundances of different phyla were calculated and display it in the bubble plot generated by package ‘ggplot2’. We investigated the pair-wise Spearman’s correlation coefficients among the major OTUs (average abundance > 0.1%), and created the network by software Gephi [46]. The number of edges connected to different phyla was summarized in R. The topological role of a node was characterized by its standardized within-module degree z and its among-module connectivity, p,

1  
2  
3  
4 using the plugin GIANT in Cytopscape [47,48]. The nodes were sorted into peripherals,  
5 connectors, module hubs, and network hubs as previously described [49].  
6  
7  
8  
9  
10  
11

### 3. Results and discussion

#### 3.1. Characterization of solely and dual nano-particles (nPs)

17 Immobilization of anaerobes degrading organics on the nano-particles (nPs) is a promising  
18 approach where the H<sub>2</sub> yield (HY) is improved due to an increase of hydrogenase enzyme as  
19 described earlier by Elreedy et al., [17]. Moreover, metal nPs represented a source of nutrients  
20 for micro-organisms at appropriate doses where Han et al., [50] found a gradual release of iron  
21 from hematite nPs in the reaction medium. Solely and dual nano-particles (nPs) i.e. graphene  
22 oxide (nGO), graphene (nG), magnetite (nM), graphene/magnetite (nG/M), hydroxyapatite  
23 (nHap) and graphene/hydroxyapatite (nG/Hap) was attempted for enhancement of hydrogen  
24 fermentative of black liquor (BL). The characteristics of solely and dual nano-particles (nPs) are  
25 presented in **Fig. 2a**. The prepared graphene nanoparticles (nG) revealed disordered structure  
26 which is reflected by the broad X-ray diffraction peaks centered at approximately 2θ of 19° which  
27 corresponds to the (002) reflection of graphene. The broad (002) peak revealed that the graphene  
28 is not crystalline as graphite as shown in **Fig. 2a**. The XRD pattern of nHap showed several  
29 signals at 2θ of 25.88°, 31.88°, 32.28°, 34.08°, 39.78° and 49.58°, corresponding to the  
30 diffraction planes (0 0 2), (2 1 1), (1 1 2), (2 0 2), (1 3 0) and (2 1 3), respectively (JCPDS no.01-  
31 073- 8417). Those signals confirmed the deposition of nHAP in a hexagonal structure.  
32  
33  
34  
35  
36  
37  
38  
39  
40  
41  
42  
43  
44  
45  
46  
47  
48  
49  
50  
51  
52  
53  
54  
55

56 Fourier transform infra-red (FTIR) spectra of nGO is illustrated in **Fig. 2a**. GO spectrum showed  
57 peaks at 1046, 1445, 1629, 2924 and 3430 cm<sup>-1</sup> as earlier reported by Kyzas et al.,[51]. The  
58  
59  
60  
61  
62  
63  
64  
65

intense, broad band at  $3430\text{ cm}^{-1}$  is attributed to O-H stretching of the hydroxyl and carboxyl groups of GO, in addition to the residual water between the GO sheets. Peaks at 1046 and  $1445\text{ cm}^{-1}$  is attributed to the stretching of epoxy group, whereas peak at  $1629\text{ cm}^{-1}$  were due to the C=O stretching in the carbonyl and carboxylic groups [28]. These hydrophilic oxygen-containing functional groups provided GO sheets highly dispensable in water, resulting formation of hydrogen bonds between the graphite and water molecules. Magnetite (nG) provided an intense peak at  $562\text{ cm}^{-1}$  which is attributed to the stretching vibrational mode due to metal-oxygen Fe-O bonds in the crystalline lattice of  $\text{Fe}_3\text{O}_4$  [52]. Bands at  $1636$  and  $3433\text{ cm}^{-1}$  are related to the hydroxyl group and confirms the presence of OH-bending and OH-stretching group, respectively. FTIR spectrum of nHap illustrated a characteristic absorption peaks (**Fig. 2a**). The broad bands were detected at  $3430$  and  $1633\text{ cm}^{-1}$  which could be attributed to the adsorbed water. Bands at peaks of  $589$  and  $1048\text{ cm}^{-1}$  were appeared for  $\text{PO}_4^{3-}$  group[53].

The SEM imaging of nG sheets are presented in **Fig. 2b**. The image showed a layered structure with a fluffy appearance and highly agglomeration of the sheets. nGO morphology under SEM micrograph showed a crumpled and rippled structure due to the deformation upon exfoliation as shown in **Fig. 2b**. The multilayered structure is clearly observed. Magnetite (nM) was appeared to be very fine powder configuration with mono-dispersed nature (**Fig. 2b**). The particles seem to be scattered with no signs of aggregation [54]. Morphology of the nHap showed a powder configuration with rod shaped nanoparticles with no evidence of agglomeration (**Fig.2b**). Energy dispersive X-ray (EDX) analysis of the nG, nGO, nM, nHap, nG/M and nG/Hap are presented in **Table 1c**. The starting molar ratio of calcium to phosphorus was (1.67) in nHap which are confirmed by the results of EDX analysis. Likely, high quantity of carbon (70.4) and low portion of oxygen (29.66) are observed for nG. The oxygen atoms were still detected in the nG sheets

structure which strongly indicates the occurring of reduction of graphene oxide into nG sheets. However, the reduction process was not fully accomplished due to the presence of other oxygen groups in the graphene structure. The atom ratio of C: O in nGO was in consistence with the original precursors which estimated to be 4:5 (0.8). The appearance of the sulfur (2.05%) in the spectrum of nGO was due to the use  $H_2SO_4$  as oxidizing agent. The EDX analysis of nM revealed pure  $Fe_3O_4$  nanoparticles where the composition analysis was 69.44% for Iron and 30.56 % for oxygen. This result demonstrates the high purity of the magnetite nanoparticles (nM). The data for composition of nG/Hap was satisfactory where carbon, oxygen, phosphorous and calcium were 28.48, 35.73, 11.34 and 24.45% respectively.

**Fig.2b** shows the transmission electron microscopy (TEM) imaging of nG, where a few layers of relatively transparent sheets was entangled and rippled with each other. nG/Hap showed the crystallization thin shape (ca. 20 nm in diameter), short in length (30–50 nm) and nano-rods with minor aggregations. The electron diffraction pattern (inset of **Fig. 2b**) showed polycrystalline diffraction rings of nG/Hap composite.

### 3.2. Impact of supplementation of solely and dual nano-particles (nP<sub>s</sub>) on the efficiency of anaerobes treating black liquor

#### 3.2.1. Hydrogen production (HP) and Yield (HY)

Nano-metals are playing a key role for hydrogen fermentative process i.e. iron (Fe) acts a serves factor for hydrogenase enzyme (HE) secretion and intercellular electron transfer. Addition of Fe concentration (18–55 mg/L) improved hydrogen yield (HY) by 1.5 fold and reduced the lag phase period by 0.33 fold [55]. The efficiency of anaerobes for HP and HY were increased due

to supply of calcium (Ca) concentration of 50–150 mg/L in the reaction medium [56]. The hydrogen fermentative of BL was comprehensively investigated by immobilization of anaerobes on the solely and dual nano-particles (nPs) as shown in **Fig. 2c**. The experimental results were closely fitted to the simulated ones with  $R^2$  ranging from 0.895 to 0.993. The hydrogen potential (P) and HY was quite low for the control batches containing only anaerobes and BL which was amounted to  $198.5 \pm 10.8$  mL and  $44.6 \pm 3.8$  mL/gCODs removed respectively. Those values were significantly ( $p < 0.05$ ) increased up to  $274.0 \pm 11.8$  mL and  $63.8 \pm 3.9$  mL/gCODs removed when the anaerobes supplemented with 10 mg/gVS nG. This was mainly due to an increase of hydrogenase enzyme (HE) activity from  $0.08 \pm 0.001$  (control) to  $0.108 \pm 0.004$  mg M.B reduced/min for anaerobes supplemented with 10 mg/gVS nG. The addition of nG facilitates the electron transfer between the substrate and anaerobes and plays a crucial role as a carrier for anaerobes creating unusual conditions for hydrogen producing bacteria (HPB). The surface area of nG is quite high to facilitate the electrons adsorption and subsequently electron transfer between nG and hydrogenase enzyme (HE) molecules to catalyze the conversion of H<sub>2</sub> to proton and vice versa. Moreover, the addition of nG increased the enzymatic activities degrading proteins and carbohydrates i.e. α-amylase, α- xylanase, CM-cellulase, and protease by values of  $44.7 \pm 1.9$ ,  $93.9 \pm 1.2$ ,  $25.0 \pm 0.9$ ,  $100 \pm 6.35\%$  respectively. Likely HY and P was increased by values of 37.6 and 34.4% for anaerobes supplemented with 10 mg/gVS nGO where the HE activity was  $0.117 \pm 0.003$  mg M.B reduced/min. The P and HY was better for anaerobes supplemented with 10 mg/gVS magnetite (nM) due to it is composed of iron which play a key role for enhancement of metabolism of hydrolytic bacteria and subsequently hydrogen production. The P values of nM exceeded by 47.5 and 123 mL as compared to nG and control samples respectively. Similar observation was recorded for HY where it was better by values of

38.4% and 44.9% as compared to anaerobes free nPs. The HY was further increased by 75.5 mL and 36.4 mLH<sub>2</sub>/gCODs removed respectively. This was mainly due to the addition of magnetite (nM) which reduced the half maximal inhibitory concentration (IC<sub>50</sub>) from 49.1±2.8 µg gallic acid equivalent/mL for BL to 15.75±2.5 µg gallic acid equivalent/mL for anaerobes supplemented with nM. Moreover, addition of magnetite to the reaction medium reduced the lag phase from 72 hrs for control to 36 h due to a high activity of HE (0.14 ± 0.003 mg M.B reduced/min). Likely, immobilization of anaerobes on Fe<sub>2</sub>O<sub>3</sub> NPs Improved HY by 57.8% (0.90 mol H<sub>2</sub>/mol glucose) from starch wastewater [57]. HY was increased by 26.4% (1.53 mol H<sub>2</sub>/mol glucose) by anaerobic sludge supplemented with 400 mg/L of Fe<sub>3</sub>O<sub>4</sub> NPs under mesophilic conditions [58]. However, 50 mg/L of Fe<sub>3</sub>O<sub>4</sub> NPs was sufficient to improve the HY by value of 83.3% (44.3 l/kg COD) by mixed culture from distillery wastewater[59]. Addition of 400 mg/L Fe-nPs to the mixed bacterial consortium fed with glucose caused a reduction of HY by 38% (1.23 mol/mol hexose) [60]. Incorporation of graphene (nG) with magnetite (nM) for immobilization of anaerobes highly improved the P and HY as shown in **Fig. 2C**. The P (211.5±10.2 mL) and HY (106 .3 ±2.7mL H<sub>2</sub>/gCODs removed ) was quite high and increased by value of 51.6 ± 2.1and 61.6±1.6% as compared to the control batch assay. A significant (P≤0.05) improvement of 24.03 % for P and 20.4% for HY was occurred due to the use of dual nano-particles (nG/M). This was mainly due to an increase of HE activity from 0.14 ± 0.003 to 0.178±0.02 mg M.B reduced/min). Moreover, the enzymatic activities of α-amylase, α- xylanase, CM-cellulase, polygalacturinase and protease were increased by 59.0±2.5, 75.2±2.6, 10±0.9, 88.5± 4.7and 95.7±10.2% respectively. The ABTS (Scavenging %) was increased from 31.9±2.9 to 89.2±0.6% with supplementation of 10 mg/gVS nG/M onto the anaerobes. This indicates that the use of dual nanoparticles would improve the antioxidant activity and enhance the HY. Likely

1  
2  
3  
4 Mostafa et al., [20] found that supplementation of anaerobes with 100 mg/L magnetite/graphene  
5 oxide (MGO) increased the HY up to  $112.4 \pm 10.5$  mLH<sub>2</sub>/gCOD<sub>removed</sub> from gelatinous wastewater  
6 and the conversion efficiency of carbohydrates, proteins and lipids was promoted up to  $80.8 \pm 7.6$ ,  
7  
8  
9  
10 times with anaerobes supplemented with hematite and nickel oxide NP as compared to control  
11 batches resulting an increase of HY by a value of 32.6% [50].  
12  
13  
14  
15  
16  
17

18  
19  
20  
21 The addition of calcium ions onto the anaerobes will maintain a high cell density in the digester  
22 and induce microbial aggregation [61]. Moreover, Ca<sup>2+</sup> would improve granulation process by  
23 facilitating early aggregation resulting large particle sizes and more biomass growth. The  
24 addition of Ca<sup>2+</sup> to the anaerobic reactor improved sludge granulation by adsorption, adhesion  
25 and multiplication process [56]. Moreover, the presence of Ca<sup>2+</sup> would enhance the secretion of  
26 extracellular polymeric substance (EPS) to keep the ionic balance in the reaction medium.  
27 Moreover, EPS are playing a key role for cell binding and agglomerate the anaerobes due to  
28 electrostatic interaction force. EPS is always negatively charged and can easily bind with  
29 positively charged organic pollutants and facilitate the metabolism process of the organic content  
30 of the BL. EPS prefer to bind with divalent ions in the reaction medium to form of more stable  
31 complexes [56]. Accordingly, the use of hydroxyapatite (nHap) rich with calcium and  
32 phosphorous ions in nano-scale was attempted here for enhancement of HP and HY from BL as  
33 shown in **Fig. 2C**. However, the P of  $335 \pm 8.7$  ml and HY of  $71.7 \pm 4.7$  ml/gCODs<sub>removed</sub> were  
34 lower than those obtained from the dual nanoparticles of (nG/M). Yuan et al., [62] found that  
35 supplementation of 100 mg/L calcium improved the cell retention, density by two-fold, hydrogen  
36 production rate (HPR) and HY of 24.5 L/d/L and 3.74 mol H<sub>2</sub>/ mol sucrose respectively.  
37  
38  
39  
40  
41  
42  
43  
44  
45  
46  
47  
48  
49  
50  
51  
52  
53  
54  
55  
56  
57  
58  
59  
60  
61  
62  
63  
64  
65

1  
2  
3  
4 Calcium ion addition of 75 - 150 mg/L enhanced the granulation process and increased HY up to  
5 3.6 molH<sub>2</sub>/mol-sucrose and HPR of 807 mmol-H<sub>2</sub>/L-d. However, the HPR and HY was  
6 deteriorated at Ca concentration of 300 mg/L [56].  
7  
8  
9  
10  
11  
12  
13

14 The dual nano-particles of nG/Hap was attempted to improve the P and HY as shown in **Fig. 2C**.  
15 The P and HY was maximized up to  $514 \pm 11.6$  mL and  $115.9 \pm 12.2$  mL /gCODs removed at a dose  
16 of 10 mg/gVS. Those values are higher than those achieved by nG/M by values of 104 mL & 9.6  
17 mL/gCODs removed and control samples by  $61.3 \pm 4.1$  and  $61.5 \pm 2.3\%$  respectively. This was  
18 mainly due to the addition of nG/Hap which enhanced and improved the secretion of EPS from  
19 222  $\pm 11.3$  to  $248 \pm 8.9$  mg/gVS and HE from  $0.178 \pm 0.02$  to  $0.28 \pm 0.004$  mg M.B reduced/min as  
20 shown in **Fig.2c**. Moreover, the lag phase period was largely reduced from 72 (control) to 12.0  
21 h., and from 24 h (nG/M) to 12 h., (nG/Hap). This indicates that addition of nanoparticles rich  
22 calcium ions accelerated the biodegradation activities and subsequently HP and HY.  
23 Furthermore, the ABTS (Scavenging %) was increased from  $31.9 \pm 2.9$  to  $89.9 \pm 0.28\%$  due to the  
24 supplementation of nG/Hap. Likely, the HY was increased by 27% due to co-addition of NPs  
25 (50 mg/l Fe<sub>2</sub>O<sub>3</sub> + 10 mg/l NiO) as compared with controls and a significant decrease of the lag  
26 phase from 3.6 to 2.8 h was occurred [63]. The HP of 150 l/kg VS was maximized at Fe and Ni  
27 concentration of 37.5 and 37.5 mg/L, respectively and the HY was improved by 200% as  
28 compared to controls[64].  
29  
30  
31  
32  
33  
34  
35  
36  
37  
38  
39  
40  
41  
42  
43  
44  
45  
46  
47  
48  
49  
50  
51  
52

### 53 3.2.2. Enzymatic assays of microbial carbohydrate and protein -cleaving

54  
55  
56 Bacterial cells cannot directly up-take the macro-molecules i.e. carbohydrates and proteins  
57 present in BL. Therefore, anaerobes produce and excrete extracellular hydrolytic enzymes such  
58  
59  
60  
61

as amylases, cellulases and proteases to breakdown and solubilize the macromolecular structures into soluble form matter i.e. simple sugars and amino acids to facilitate transport of substrate into the cell membrane[65]. Those simple by-products are utilized by anaerobes to gain energy and synthesize new cellular components. Polysaccharides are converted into simple sugars. Hydrolysis of cellulose is taken place by the cellulase enzyme to yield glucose while starch is converted into glucose by amylase enzymes[66]. The hydrolysis process is normally rate-limiting step for anaerobes degrading substrate containing high fractions of particulate organic matter. Fortunately, the major portions of organics in the BL were in the soluble form (98%). Understanding of hydrolytic enzyme production, activities and its relations with nanoparticles supplementation are deeply discussed here. Enzymatic activities are the key of transformations of high molecular weight (HMW) organics into simple components to be easily utilized by anaerobes, i.e. conversion of proteins and carbohydrates into amino acids and glucose respectively. Those metabolites are further converted by acidogenesis into volatile fatty acids (VFAs) and hydrogen gas. The BL contained a high protein and soluble carbohydrate content of  $11.36 \pm 0.46$  g/l and  $43.5 \pm 12.7$  g/l which needs to be hydrolyzed by anaerobes. Direct protein uptake by anaerobes is impossible and requires extracellular enzymes i.e. proteases to cleave HMW proteins into amino acids and peptides which can subsequently utilize and metabolize by acidogenesis into VFAs, sulfide, H<sub>2</sub> and ammonia [67]. Likely, hydrolysis of carbohydrates needs particular enzymes i.e.  $\alpha$ -amylase,  $\alpha$ - xylanase, CM-cellulase and polygalacturonase for metabolism process. **Fig. 2d** shows the enzymatic activities of proteases,  $\alpha$ -amylase,  $\alpha$ - xylanase, CM-cellulase and polygalacturonase which was strongly dependent on the type of nano-particle (nPs) addition. The enzymatic activities of  $\alpha$ -amylase,  $\alpha$ - xylanase, CM-cellulase and protease was  $31.5 \pm 2.4$ ,  $4 \pm 0.2$ ,  $7.5 \pm 1.2$  and 0 for control samples which was significantly ( $P \leq 0.05$ )

increased up to  $57 \pm 2.1$  and  $69 \pm 2.3$  U/100ml,  $66.5 \pm 2.7$  and  $116 \pm 11.2$  U/100ml,  $10 \pm 0.2$  and  $14.5 \pm 0.34$  U/100ml,  $335 \pm 11.7$  and  $155 \pm 4.3$  U/100ml in the batches supplemented with nG and nGO respectively (**Fig.3a**). Polygalacturinase activity was increased from 0 (nG) to  $47.5 \pm 1.3$  U/100ml for the samples containing nGO. This strongly indicates that the enzymes activities are promoted due to the supplementation of the anaerobes with nG and nGO. Amylase activity was quite high during mesophilic anaerobic digestion of solid potato waste compared to other hydrolases due to the existence of amylolytic microbes [66]. However, the enzymatic activities were significantly improved with the addition of dual nanoparticles i.e nG/M and nG/Hap as shown in **Fig.3a**. The enzymatic activities of  $\alpha$ -amylase,  $\alpha$ - xylanase, CM-cellulase, polygalacturonase and protease were  $57 \pm 2.3$ ,  $66.5 \pm 4.3$ ,  $14.5 \pm 0.5$ ,  $59 \pm 4.5$ ,  $165 \pm 8.7$  and  $112 \pm 11.2$  U/100ml for anaerobes supplied with nG and increased up to  $77 \pm 2.3$ ,  $131 \pm 3.2$ ,  $35 \pm 1.2$ ,  $291 \pm 12.5$  and  $740 \pm 23.7$  U/100ml for nG/M. Supplementation of iron source onto the reaction medium enhanced and promoted the enzymes activities, hydrolysis and subsequently the HY (**Fig.3a**). Further promotion of enzymatic activities were occurred due to supplementation of graphene/hydroxyapatite (nG/Hap) where the  $\alpha$ -amylase,  $\alpha$ - xylanase, CM-cellulase, polygalacturonase and protease were increased by values of 52.5, 26.4, 32.7, 0.7 and 29.2 respectively. H<sub>2</sub> production was increased by 60–70% due to inoculation of digester with external hydrogen-producing bacteria with cellulolytic activity (*Caldicellulosyruptor saccharolyticus*) [68]. Feng et al., [69] found that addition of 20 g/L Zero valent iron increased the activities of protease and cellulase up to 92.0 and 91.7%, respectively. Similar results were observed for extracellular polymeric substances (EPS) as shown in **Fig.2c**. Hydrolytic enzymes i.e. cellulase and pronase E caused a reduction of 80% for solids and 93% removal of particulate COD [70] and the addition of  $\alpha$ -amylase (0.06 g/g dry sludge) increased the hydrolysis rate constant from 0.106 to 0.215 h<sup>-1</sup> and the activation energy

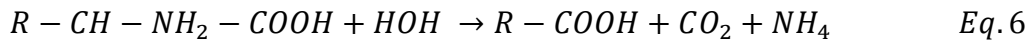
for hydrolysis of volatile solids was reduced from 62.72 kJ/mol (control sample) to 20.19 kJ/mol ( $\alpha$ -amylase treatment)[71]. The EPS was  $23 \pm 11$  mg/gVS for fermented sludge and increased up to  $78 \pm 22$  mg/gVS for fermentation of BL and sludge. Addition of substrate promoted the anaerobes to generate the EPS to enrich the reaction medium and agglomerate the bacterial cells for degradation of organics. Furthermore, the EPS generation was substantially enhanced due to enrich the anaerobes with solely and dual nano- particles (**Fig.2c**). Better EPS generation was recorded based on the following order nG/Hap>nG/M>nM>nHap> nGO > nG. The maximum EPS generation of  $248 \pm 30$  mg/gVS was recorded for immobilization of anaerobes on the nG/Hap due to the presence of calcium ions. The presence of Ca ions increase the cell retention, and catalytic activity of anaerobes[72]. Morgan et al.,[73] found that the addition calcium onto the anaerobes promotes extracellular polysaccharide constituents which utilized for cell bindings with the substrate. Addition of 150 mg-Ca<sup>+2</sup>/L reactor provided the highest EPS values of the digester producing hydrogen from sucrose [56].

### 3.2.3. Protein, carbohydrate conversion and ammonification process

The anaerobes supplemented with solely and dual nanoparticles provided a significant positive impact on the protein and carbohydrate degradation (**Fig.3b**). The conversion of protein and carbohydrate was 1.0 and 1.22 g/l for control sample which was significantly increased up to 1.93 and 1.2 g/l for anaerobes supplemented with nM and to 2.7 and 1.5 g/l for nG/Hap samples. This can be attributed to a higher protease,  $\alpha$ -amylase and  $\alpha$ - xylanase activities and lower IC<sub>50</sub> in the batches supplemented with nG/Hap. Likely, Feng et al. [69] found that the degradation efficiency of protein and carbohydrate was increased from 59.1to 67.8% and from 32.3% to 43.4% using anaerobes immobilized on zero valent iron. Likely, the HY of  $106.3 \pm 11.6$

mL/gCODs removed,  $190 \pm 8.9$  mL/g carbohydrate removed ,  $339.4 \pm 13.9$  mL H<sub>2</sub>/g protein removed based on CODs, carbohydrate and protein conversion was quite high for anaerobes supplemented with nG/M and increased up to  $115.9 \pm 12.6$  mL/gCODs removed,  $190.6 \pm 9.8$  mL/g carbohydrate removed and  $365.4 \pm 14.3$  mL H<sub>2</sub>/g protein removed for nG/Hap. However, Yang et al., [74] found that carbohydrate was more efficiently anaerobically biodegraded than protein resulting removal efficiencies of 49.7% and 32.2%, respectively.

Protease is essential enzyme for protein hydrolysis to form amino acids which subsequently metabolized to generate NH<sub>4</sub><sup>+</sup> in the reaction medium. The protease enzyme activities were quite high for anaerobes supplemented with nG/Hap which mitigated the known limiting step of protein decomposition. Accordingly, proteases enzyme activity is very important factor for ammonification. Ammonification process is occurred due to chemical reaction in which NH<sub>2</sub> groups are converted into ammonium (NH<sub>4</sub><sup>+</sup>) and/or the N-org. is anaerobically converted into ammonia (**Eqs. 6 and 7**).

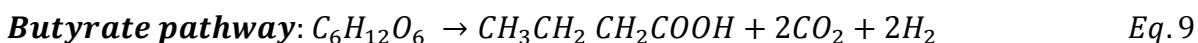


The relationship between the ammonification process and protease enzyme activity are presented in **Fig. 3b** where the ammonification process was the optimum for anaerobes supplemented with nG/Hap. The ammonification process was optimized in the batches supplemented with dual nanoparticles i.e. nG/M and nG/Hap where, the ammonia was increased in the reaction medium by values of -17% and -18% respectively. These values were higher than those obtained for solely nanoparticles i.e. -2.4%, - 5.5%, -10.5 and -11% for the anaerobes supplied with nG, nGO,

nM and nHap respectively. This was mainly due to the conversion of nitrogen (TKj-N) was quite high for the batches containing dual nanoparticles. TKj-N removal efficiency was 17.2% for nG, 25.3% for nGO, 26.5% for nM, 28.8% for nHap which was significantly increased up to 33.5% for nG/M and 34.7% for nG/Hap as shown in **Fig. 3b**.

#### 3.2.4. Metabolite by-products

Hydrolysis is the conversion of macro-molecules i.e. carbohydrates and proteins into simple sugars and amino acids by extracellular enzymes which secreted in the reaction medium by anaerobes. Therefore, the hydrolysis rate is mainly dependent on the substrate type and enzymes activities. The acidogenesis process is employed for biodegradation of amino acids and sugars into volatile fatty acids (VFAs), H<sub>2</sub>, H<sub>2</sub>S and ammonia (NH<sub>4</sub>-N). The acidogenesis process of BL was accompanied by dropping in the pH value of the reaction medium due to the production of acetate (HAc), Iso-butyrat (Iso-HBu) and Valerate (HVa). The pH for all samples was dropped from 7.5±0.2 to the minimum value of 6.8 ±0.2 in case of the batches supplemented with solely and dual-nanoparticles. Theoretically, conversion of organics into HAc and HBu produces 4 and 2 mol of H<sub>2</sub> respectively (**Eqs. 8 and 9**). Production of propionate (Hpr) would consume the H<sub>2</sub> gas which should be avoided (**Eq.10**)[75]. Acetate fermentation pathway is prevailed at HAc to HBu ratio > 1 (**Eq. 8**) and HAc/HBu < 1 provides butyrate fermentation pathway (**Eq. 9**).



The results in **Fig 3c** show the impact of supplementation of solely and dual – nanoparticles on the VFAs production in terms of valerate (HV<sub>a</sub>), iso-butyrate (iso-HBu), propionate (HPr), formate (HFo) and acetate (HAc) in the reaction medium. The fermentation of the inoculum sludge (S) was carried out as a control where, iso-butyrate (iso-HBu), propionate (HPr), formate (HFo) and acetate (HAc) was increased in the reaction medium up to  $38.6 \pm 2.6$  mg/L,  $21.4 \pm 0.1$  mg/L,  $21.3 \pm 7.9$  mg/L and  $19.9 \pm 0.1$  mg/L respectively. The HV<sub>a</sub>, iso-HBu, HPr, HFo and HAc was  $3200 \pm 212$  mg/L,  $1244 \pm 100$  mg/L,  $267 \pm 12.9$  mg/L,  $344 \pm 10.9$  mg/L and  $653 \pm 22.8$  mg/L in the control sample which was significantly increased up to  $10259 \pm 123$ ,  $1628.6 \pm 78$ ,  $288.1 \pm 11.9$ ,  $927.8 \pm 8.8$  and  $1465.3 \pm 11.9$  for nG and to  $3312 \pm 108$ ,  $1261 \pm 66$ ,  $344 \pm 10.9$ ,  $340 \pm 9.8$  and  $733 \pm 10.8$  mg/L for nGO. The H<sub>2</sub> production was low in the control samples due to the propionate (HPr) production in the reaction medium which consume the hydrogen and converted into acetate. The HY and HP was higher in the samples rich with nG and nGO than those achieved for control samples due to a higher production of HAc and Iso-HBu. However, butyrate fermentation pathway was dominant for the control, nG and nGO where the HAc/Iso-HBu ratio was 0.52, 0.9 and 0.58 respectively. Engliman et al., [76] found that the HAc was maximized at a level of 32 mM at increasing iron NPs concentrations from 0 to 500 mg/L and acetate fermentation pathway was the major degradation mechanism. Moreover, the metal NP concentration was not consumed by the anaerobes and remained unaffected after the fermentation period. 200 mg Fe<sub>2</sub>O<sub>3</sub> NP/L achieved maximum acetic acid of 13.57 mM and butyric acid of 31.21 mM from hydrogen fermentative of complex distillery wastewater as a substrate [64]. HAc and HBu concentrations was significantly increased with the addition of hematite nanoparticles to the anaerobes compared with the corresponding control test[50]. Acetate (HAc) fermentation pathway was dominant for the samples supplemented with nM and nHap where the HAc was  $344.3 \pm 8.9$  and

1  
2  
3  
4 2005.2 ±10.2 mg/L respectively and the iso-BUt was absent in the digestate. However, the HPr  
5 production was quite high and amounted to 1294.9±11.9 and 1547.7±11.9 mg/L in the reaction  
6 medium resulting a drop in the HY and HP. The HP and HY was quite high for the samples  
7 containing dual nanoparticles i.e. nG/M and nG/Hap due to the dominance of acetate  
8 fermentation pathway and lower production of HPr in the digestate. The HVa, iso-HBu, HPr,  
9 HFo and HAc was 3875±89, 1514±56, 276±12.9, 367±11 and 1812±16.2 mg/L in the digestate  
10 of the sample containing nG/M with HAc/iso-But ratio of 1.2. Iso-butyrat was absent in the  
11 samples containing nG/Hap indicating the acetate fermentation pathway resulting residual values  
12 of 12407.5±211 mg/L for HVa, 1042.8±11.2 mg/L for HPr, 107.2±9.8 mg/L for HFo and  
13 527.3±11.8 mg/L in the digestate. Co-addition of NiO NP, the Fe<sub>2</sub>O<sub>3</sub> NP provided the maximum  
14 production of 39.60 mM for butyric acid and 15.23 mM for acetic acid from anaerobic  
15 digestion of complex distillery wastewater [64]. HAc concentration was significantly increased  
16 from 705.31 ± 56.20 to 1229.22 ± 86.47 mg/L in the bulk liquid of anaerobic fermentation of  
17 petrochemical wastewater industry at increasing the dosage of nNi/G from 0 to 60 mg/L  
18 respectively[17].

40  
41  
42  
43 3.2.5.Total phenolic compounds (TPC), total reducing sugars (TRS), the half maximal  
44 inhibitory concentration (IC<sub>50</sub> -µg gallic acid equivalent/mL) and antioxidant activity  
45  
46 –ABST Scavenging %)

47  
48  
49  
50  
51 The BL contains total reducing sugars (TRS) of 262.8±11.9 mg/L which are mainly glucose and  
52 fructose fractions. Those mono-saccharides are further biodegraded by acidogenesis process as  
53 shown in **Fig. 3d** and reported earlier by [77]. The results showed that the TRS removal was  
54 increased in the samples supplemented with solely and dual-nanoparticles. The TRS removal  
55  
56 increased in the samples supplemented with solely and dual-nanoparticles. The TRS removal  
57  
58 increased in the samples supplemented with solely and dual-nanoparticles. The TRS removal  
59  
60 increased in the samples supplemented with solely and dual-nanoparticles. The TRS removal  
61  
62 increased in the samples supplemented with solely and dual-nanoparticles. The TRS removal  
63  
64 increased in the samples supplemented with solely and dual-nanoparticles. The TRS removal  
65

efficiency was maximized at levels of  $65.4 \pm 1.2$  and  $68.2 \pm 1.3$  % for the anaerobes supplemented with nG/M and nG/Hap respectively. Antioxidants could be natural phenolic compounds (tocopherols, flavonoids, and phenolic acids), nitrogen compounds (alkaloids, chlorophyll derivatives, amino acids, and amines), or carotenoids as well as ascorbic acid [34]. The polyphenols are very strong antioxidant compounds causing de-oxygenation of the waters [78]. The results in **Fig. 3d** clearly show the relationship between the antioxidant activities ABTS-scavenging (%) and the total phenolic compounds (TPC) content. The antioxidant activity ABTS-scavenging (%) was increased from  $31.9 \pm 2.9$  (initial) to  $89.2 \pm 0.6$  for nG/M and to  $89.8 \pm 0.3$  for nG/Hap. This was mainly due to a drop of TPC from  $171.8 \pm 12.4$  mg/100mL (initial) to  $90.5 \pm 20.5$  mg/100mL for nG/M and to  $93 \pm 2.8$  mg/100mL for nG/Hap (**Fig. 3d**). Apparently, immobilization of anaerobes on the dual -nanoparticles mitigated the inhibition effect of TPC and increased the antioxidant activity which subsequently enhanced the HY and HP. Likely, [78] found that the antioxidant activity and phenolic compounds are inversely proportional relationship. The removal efficiencies of TPC were  $36.3 \pm 0.3\%$  for nG,  $38.3 \pm 0.7\%$  for nGO,  $38.9 \pm 0.9\%$  for nM and  $43 \pm 1.2\%$  for nHap. Those values were slightly increased for dual nanoparticles i.e.  $47.3 \pm 1\%$  for nG/M and  $45.9 \pm 1.2\%$  for nG/Hap. Likely, Hernandez and Edyvean [79] achieved the maximum biodegradation of phenolic compound of  $63.85 \pm 2.73\%$ , by anaerobes. However, the inhibition of methanization was occurred at high influent phenolic compounds of 800 and 1600 mgTPC/L.

The black liquor (BL) contains phenolic compounds of  $171.8 \pm 12.4$  mg/100mL which resulted from chemical pulping of agriculture waste components. The presence of phenolic compounds in the substrate would inhibit the anaerobes and subsequently decrease the H<sub>2</sub> generation where the

half maximal inhibitory concentration  $IC_{50}$  ( $\mu$ g gallic acid equivalent/mL) was accounted for  $49.1 \pm 2.8$   $\mu$ g gallic acid equivalent/mL for initial substrate (**Fig. 3d**). The  $IC_{50}$  was significantly dropped to  $16.4 \pm 1.1$   $\mu$ g gallic acid equivalent/mL due to immobilization of anaerobes on the nG and the total phenolic compounds were removed by value of  $36.2 \pm 0.3$  %. Moreover, the  $IC_{50}$  was further decreased up to  $15.7 \pm 2.5$   $\mu$ g gallic acid equivalent/mL for anaerobes supplemented with nM due to the removal of phenolic compounds ( $38.9 \pm 0.9$ %).  $IC_{50}$  was minimum i.e.  $14.7 \pm 0.6$  and  $13.1 \pm 2.7$   $\mu$ g gallic acid equivalent/mL for dual nanoparticles (nG/M and nG/Hap) respectively. This indicates that supplying of solely and dual nano-particles onto the anaerobes degrading BL substantially promotes the antioxidant and enzymatic activities, reduces the inhibition  $IC_{50}$  effect of the phenolic compounds and surprisingly enhanced the hydrogen yield and production.

### 3.2.6. Fate of organics (aromatics, alkanes, alkenes, alcohols, esters ) and nano-particles after fermentation process

The fate of nG/Hap after fermentation of 14 days was examined by XRD pattern, FT-IR, SEM and EDX analysis (**Fig. 4**). The XRD pattern shows the peaks intensity, crystallinity index (CI) and diffraction plane of the control and anaerobes supplemented with nG/Hap. The CI was decreased from 45 to 29.9% after fermentation with nG/Hap indicating that addition of nG/Hap reduced the CI of the feedstock and facilitate the hydrogen production. Moreover, the main broad diffraction peak (0.10) was observed at  $2\Theta$  of  $26.585^\circ$  with d-space of  $3.35021$   $\text{\AA}^\circ$  for control sample which was shortened with the addition of nG/Hap to 0.11 at  $2\Theta$  of  $26.664^\circ$  with d-space of  $3.34050$   $\text{\AA}^\circ$ . A new board diffraction peak (0.065) was appeared at  $2\Theta$  of  $50.163^\circ$  with d-space of  $1.81715$   $\text{\AA}^\circ$  due to the addition of nG/Hap onto the reaction medium. Moreover a

number of diffraction peaks was disappeared in the samples containing nG/Hap and new peaks were detected indicating the biological activities of the anaerobes immobilized on nG/Hap. However, the XRD pattern of nHap showed several signals at  $2\theta$  of 26.664, 29.45, 30.83, 31.29, 31.84, 50.163, 59.95 and 68.187°, corresponding to the diffraction planes (0 0 2), (2 1 1), (1 1 2), (2 0 2), (1 3 0) and (2 1 3), respectively (JCPDS no.01-073- 8417)[80]. Those signals confirmed the presence of nHAP in the digestate after fermentation process and the nG/Hap was not up-taken by anaerobes as described earlier by Han et al., [50].

The FTIR results of the control and anaerobes loaded with nG/Hap are illustrated in **Fig. 4**. The results showed that fermentation of BL with nG/Hap largely changed the peaks intensity and height. Moreover, the peak at frequency of 878.417cm<sup>-1</sup> was stretched and increased in the samples supplemented with nG/Hap indicating the presence of  $\beta$ -glucosidic bonds between sugars and the degradation of cellulosic materials was not occurred. However, the peak of 610.36 cm<sup>-1</sup> was shifted to 588.896 cm<sup>-1</sup> and the intensity was quite low where the aromatic compounds were partially biodegraded. The intensity and the height of the peak of alcohols and phenols groups (O-H) was shortened and shifted from 3428.81cm<sup>-1</sup> (control sample) to 3427.85 cm<sup>-1</sup> in the sample containing nG/Hap indicating the degradation of compounds containing O-H groups by anaerobes. Likely the peak of 2976.59 cm<sup>-1</sup>(control sample) was shifted to 2974.66 cm<sup>-1</sup> in the sample containing nG/Hap and the latter was almost disappeared due to the biodegradation of C-H methyl and methylene groups. C=O ketone group and C-H vibration of aromatic ring was shifted from 1636.3 to 1635.34 cm<sup>-1</sup> and from 1420.32 to 1417.42 cm<sup>-1</sup> respectively due to a highly degradation process for the fermented samples with nG/Hap. The peak intensity of 1047 cm<sup>-1</sup> was detected due to the presence of C-O-C and PO<sub>4</sub><sup>3-</sup> in the reaction medium. C=O

functional groups for amides, ketone and peptic bond of protein was slightly observed in the control samples at  $610.36\text{ cm}^{-1}$  and  $588.896\text{ cm}^{-1}$  for supplemented samples with nG/Hap. The latter peak ( $588.896\text{ cm}^{-1}$ ) is mainly for asymmetric bending vibration of  $\text{PO}_4^{3-}$  which strongly indicates the presence of nG/Hap in the reaction medium [80].

Scanning electron microscopy (SEM), and energy dispersive X-ray (EDX) of sludge (S) +black liquor (BL) +nG/Hap before and after fermentation are presented in **Fig.4 and Table 2**. The results of SEM images show the sludge was incorporated with nG/Hap where the mixture was highly agglomerated due to Ostwald ripening [53,80]. The spherical shaped particles are appeared and clumped distributions are observed[80]. The results in **Table 2** show the EDX analysis of the sludge (S) +black liquor (BL) +nG/Hap before and after fermentation. The results revealed that the carbon (C) % was decreased from 58.2 to 41.85% after fermentation and the ratio of oxygen (O)/carbon (C) was increased from 0.74 to 0.95. The phosphorous and calcium was detected in the digestate after fermentation period of 14 days which indicates that the nG/Hap was not consumed by anaerobes and played a key role for catalytic activity of microbes.

**Figs. S1, S2, S3, S4 and S5 and Table 3** show GC-mass analysis of the control sample (S+BL) before and after fermentation as well as the batches containing nGO, nM, nG/Hap. The results revealed that the anaerobes immobilized on nG/Hap had the capability to remove saturated hydrocarbons in terms of docosane, tridecane, undecane, octadecane,3-ethyl-5-( 2-ethylbutyl), pentacosane, heptadecane, hexadecane,1,1bis-(dodecyloxy)- , nonacosane, dodecane, 2,2,4,9,11,11-hexamethyl, octadecane, 5,14-dibutyl-, heptadecane, 9-hexyl, tetra-cosa-methyl-cyclodo decasiloxane ,cyclodecasiloxane, eicosamethyl, and eicosamethylcyc lodecasiloxane.

The anaerobes have the capability to utilize n-alkanes as carbon and energy sources in the presence of electron acceptors [81]. Mesophilic alkane-degrading sulfate-reducers i.e. *Desulfococcus/Desulfatibacillum* cluster including *Desulfococcus oleovorans Hxd3; strain Pnd3*, *Desulfatibacillum alkenivorans AK-01* and *Desulfatibacillum aliphaticivorans CV2803T* was reported by Cravo-laureau et al., [82] for elimination of saturated hydrocarbons ranging from C12 to C20. The degradation mechanism is mainly carboxylation or fumarate. However, the latter depends on glycyl radical enzymes which yields alkyl-substituted succinate appear to facilitate the anaerobic attack of alkanes under various redox conditions [81]. Likely, the anaerobes supplemented with nG/Hap were efficient for removal of n-Alkenes, esters compounds and alcohols. 1-Hexadecene was completely eliminated in the reaction medium indicating the efficiency of anaerobes for n-Alkenes degradation. The mineralization of hexadec-1-ene by anaerobes was reported by Cravo-laureau et al., [82]. However, the pure strains capable of degrading alk-1-enes (> C23) is not existed. The main esters compounds of 1,2-benzenedicarboxylic acid, di-butyl ester, and 1,2-benzenedicarboxylic acid, butyl octyl ester was completely eliminated in the batches containing nG/Hap. Anaerobic degradation of butyl benzyl phthalate (BBP) by anaerobic bacteria in pure culture has not been reported yet [83]. The poor mineralization property of phthalates by anaerobes may be due to their high hydrophobicity and low solubility, which cause phthalates to be entrapped/adsorbed onto biomass instead of biodegradation [84]. Pulping process of rice straw produced a number of alcohols namely 2-undecanol,2-dodecanol, and tri-decanol which was absent after fermentation process as shown in

**Table 3.** This indicates the efficiency of anaerobes immobilized on nG/Hap for degradation of BL containing alcohols. However, those compounds could be useful for industrial application

which needs further investigation. Isopropyl myristate was removed only in the batches rich nG/hap as shown in **Table 3**.

### 3.3. Microbial community

#### 3.3.1. Bacterial $\alpha$ -diversity and community structure

A total number of 145,551 effective sequences were obtained for anaerobes supplemented with nG/Hap, nG/M, nM, and nHap (ranging from 30,881 to 39,873 across all samples). As shown in **Figs 5a-b**, the anaerobes supplemented with nG/Hap displayed the highest species richness compared to the other samples, while those supplemented with nHap showed the lowest ACE and Chao1. Meanwhile, we observed higher species evenness in the anaerobes exposed to dual nano-particles (nG/Hap and nG/M) as compared to solely nano-particles (nM and nHap) based on the Simpson and Shannon indices (**Figs 5c-d**). Such results indicated that the dual nano-particles increased the biodiversity of the anaerobes where specific bacteria became dominate in the population immobilized on dual nanoparticles (N1) and disappeared with solely nanoparticles i.e. nHap and nM (N3 and N4). Previous study demonstrates that biodiversity acts as the insurance of community productivity [85] which may be the reason why anaerobes immobilized on dual nanoparticles enjoyed the highest HY.

The results in **Fig. 5e** show the taxonomy of the samples harvested from batches containing nG/Hap, nG/M, nM and nHap (N1,N2,N3 and N4) to assess the variations of consortium and its relation with the biodegradation process. Data displayed that all samples (N1,N2,N3 and N4) were dominated by the phyla *Proteobacteria* (average 34.53%), *Firmicutes* (average 27.55%), *Chloroflexi* (average 10.19%), *Actinobacteria* (average 9.44%), *Planctomycetes* (average 6.64%), and *Bacteroidetes* (average 3.82%). Therein, the relative abundances of *Proteobacteria*

1  
2  
3  
4 and *Actinobacteria* were relatively lower in the anaerobes immobilized on dual nanoparticles  
5 (N1 and N2) than those on solely nHap and nM (N3 and N4). In contrast, the addition of solely  
6 nanoparticles was found to increase the abundances of *Chloroflexi* and *Bacteroidetes*. However,  
7 no substantial difference was found in the common hydrogen producers, i.e., *Firmicutes*,  
8 between the sludge immobilized on dual and solely nanoparticles.  
9  
10  
11  
12  
13  
14  
15  
16  
17  
18  
19 3.3.2. Network analysis  
20  
21  
22 The bacterial interaction network of anaerobes are illustrated in Fig. 6. The network consisted of  
23 13 modules, which largely varied in size and shape. The largest module contained 56 species,  
24 while only one specie is detected in the smallest modules. Meanwhile, the topological roles  
25 analysis (**Fig. 6b**) showed that only 7.0 OTUs were peripherals, while the remaining 127 OTUs  
26 were the connectors. No module or network hub was identified. Such result suggested the  
27 blurring boundaries among the modules and the effects of external perturbations on one OTUs  
28 can spread to the other OTUs in the network [49]. As such, the responses of community  
29 members to nanoparticles exposure should affect the hydrogen producers. As shown in Fig. 6c,  
30 the *Firmicutes* were more likely to negatively correlate with the *Actinobacteria*. With regard to  
31 the *Bacteroidetes* and *Chloroflexi*, they were more likely to co-occur with the *Firmicutes*.  
32 Moreover, we observed the same numbers of positive and negative edges between *Firmicutes*  
33 and *Proteobacteria*, suggesting that the latter can either promote or inhibit the hydrogen  
34 producers. Upon exposure to dual nanoparticles, the *Actinobacteria* were inhibited but more  
35 *Bacteroidetes* and *Chloroflexi* were observed as compared to those immobilized on solely  
36 nanoparticles. Therefore, it is expected that the dual nanoparticles can neutralize the competition  
37 and promote the metabolic cooperation in community for *Firmicutes*, and thus increased the HY.  
38  
39  
40  
41  
42  
43  
44  
45  
46  
47  
48  
49  
50  
51  
52  
53  
54  
55  
56  
57  
58  
59  
60  
61  
62  
63  
64  
65

1  
2  
3  
4     3.4. Bio-char production, net gain energy and profits  
5  
6  
7

8     The digestate resulted from fermentation of S+BL+ nG/Hap was burnt at temperature of 550 °C  
9     to harvest the bio-char. The proportions of carbon (C), nitrogen (N), oxygen (O), phosphorus (p)  
10    and potassium (K) and micro-nutrients was characterized by diffractometry of X- rays;  
11    functional groups by infrared absorption spectroscopy (FTIR) and scanning electronic  
12    microscope (SEM) (**Fig. 7a**) and **Table 4**. The results showed that the bio-char contained  
13    13.73% for C, 11.98% for Na, 1.72% for K and 6.48% for P. The O/C ratio of 2.73 was quite low  
14    indicating a high degree of condensation and structures with aromatic rings which are  
15    responsible for chemical stability of the biochar, thus increasing resistance to microbial  
16    degradation in the soil [86]. The SEM analysis showed that the bio-char was mainly white/grey  
17    in color and had a surface area of  $2.4 \pm 0.95 \text{ m}^2/\text{g}$ , density of  $1.63 \pm 0.18 \text{ g/cm}^3$ , pore volume of  
18     $0.2 \pm 0.06 \text{ cm}^3/\text{g}$ . The bio-char yield was 33±5.2%.

19  
20  
21  
22  
23  
24  
25  
26  
27  
28  
29  
30  
31  
32  
33  
34  
35  
36

37     Diffractometry of X- rays of the resulted bio-char are presented in **Fig.7c** where a peaks of  
38     kaolinite (7.14, 3.58, 2.34 Å), quartz (3.33, 4.27, 2.28, and 1.82 Å), and hematite (1.44 and 1.83  
39     Å) were detected. Moreover, a peaks characteristic of goethite (3.38, 4.20, 2.45, 2.14 Å) and  
40     calcite (3.80, 2.28, and 2.10 Å), were observed. The CI of the bio-char was 27.7%. Sharp peaks  
41     in the sample indicated the presence of various inorganic elements such as silica (Si), which are  
42     mainly related to the crystalline forms of bio-char [87]. Four broad peaks were observed at the 20  
43     value of 9°, 26.713°, 34.136° and 35.073°. The peaks at 2θ (20.78°, 26.713°, 27.75°, 31.80°)  
44     referred to the stacking structure of aromatic layers i.e. graphite 002 which originated from the  
45     small dimensions of crystallites perpendicular to aromatic layers [88]. Moreover, a sharp, non-  
46     labeled peaks presented in the bio-char indicating miscellaneous of inorganic components (Si,  
47  
48  
49  
50  
51  
52  
53  
54  
55  
56  
57  
58  
59  
60  
61  
62  
63  
64  
65

P,K,Mg). The sharp and the strongest peak at 20 of 26.713° is mainly originated from crystalline SiO<sub>2</sub> and confirmed heterogeneous surface of bio-char [89].

Carbonization process could increase aromatic structures and polymerization of the resulted bio-char. However, only five peaks were observed at wavenumbers of 3449.45, 1635.31, 1045.67, 571.05 and 458.19 cm<sup>-1</sup> (**Fig. 7b**). A peak was observed at wave length number of 3449.45 cm<sup>-1</sup> for compounds containing O-H group where hydrogen bonded -OH is stretched due to the presence of phenolic compounds[87]. A small peak was detected at wave length number of 1635.31 cm<sup>-1</sup> due to the presence of amide group and C=C of the Cis-unsaturated alkenes. A big and sharp peak was detected at 1045.67 cm<sup>-1</sup> for C-O bonds indicating the presence of the alcohol and ester group. The vibrations of the aromatic groups were occurred at frequency of 571.05 and 458.19 cm<sup>-1</sup> (**Fig.7b**). A sharp peak at 458.19 cm<sup>-1</sup> indicated the presence of silica in the bio-char which confirmed by the results of EDX and XRD analysis.

The net energy and profits gained from hydrogen fermentative and bio-char production from black liquor (BL) was briefly assessed. The energy consumption for hydrogen production (E<sub>H2</sub>) form BL was accounted for 2.75 Kj/d. The calculated net energy gain from hydrogen production is 5.5 Kj/L based on the maximum hydrogen production of 514.5 mL. The calculated energy consumption for mixing was 0.7 Kj/L and the calculated net energy gain was 2.04 Kj/L BL which equivalent to 1.10 \$/L feedstock. Those values are higher than those obtained by Soltan et al., [90] where the net energy gains were 1.09 kJ/gfeed-stock from hydrogen fermentative of 50% pea + 50% banana. The profits from bio-char should be added to evaluate the total energy gained from the fermentation and pyrolysis process. Bio-char price varied from 0.09 to 8.85

1  
2  
3  
4     \$/kg [91]. Accordingly the total profit from hydrogen fermentative and bio-char production is  
5 calculated to be 3.0 \$/L. A higher gain profits were recorded by Soltan et al., [90] where the  
6 combination of fermentation and pyrolysis processes of vegetables and fruits peels provided 5.21  
7  
8  
9     \$/kgfeedstock.  
10  
11  
12  
13  
14  
15

#### 16     **4. Conclusions** 17 18 19

20     Hydrogen fermentation of black liquor (BL) is a promising approach from economic and  
21 environmental point of view. Immobilization of solely and dual nanoparticles on anaerobes  
22 enhanced the HY and mitigate the inhibition effect of phenolic compounds. The dual nano-  
23 particles of nG/Hap provided P and HY of  $514 \pm 11.6$  mL and  $115.9 \pm 12.2$  mL /gCODs removed  
24 which are higher than those achieved by nG/M by values of 104 mL & 9.6 mL/gCODs removed and  
25 control samples by  $61.3 \pm 4.1$  and  $61.5 \pm 2.3\%$  respectively. This was mainly due to an increase of  
26 EPS from  $222 \pm 11.3$  to  $248 \pm 8.9$  mg/gVS and HE from  $0.178 \pm 0.02$  to  $0.28 \pm 0.004$  mg M.B  
27 reduced/min for nG/M and nG/Hap respectively. The HY was maximized for anaerobes  
28 supplemented with nG/M and nG/Hap due to the dominant of acetate fermentation pathway  
29 where the HAc was  $344.3 \pm 8.9$  and  $2005.2 \pm 10.2$  mg/L respectively and the iso-But was absent  
30 in the digestate. The phosphorous and calcium was detected in the digestate after fermentation  
31 period of 14 days which indicates that the nG/Hap was not consumed by anaerobes and played a  
32 key role for catalytic activity of microbes. The bio-char contained 13.73% for C, 11.98% for Na,  
33 1.72% for K and 6.48% for P. The O/C ratio of 2.73 was quite low indicating a high degree of  
34 condensation and structures with aromatic rings which are responsible for chemical stability of  
35 the bio-char, thus increasing resistance to microbial degradation in the soil.  
36  
37  
38  
39  
40  
41  
42  
43  
44  
45  
46  
47  
48  
49  
50  
51  
52  
53  
54  
55  
56  
57  
58  
59  
60  
61  
62  
63  
64  
65

1  
2  
3  
4  
5  
6  
7  
**Acknowledgements**

8 The authors are very grateful to Science Technology Development Fund (STDF) (Project ID:  
9 26271, 41591), Academy of scientific research and technology (ASRT) (Code: Call no.  
10 2/2019/ASRT-Nexus) and Imhotep project for partially financially support the research. The last  
11 author is grateful for the National Research Centre for partially supporting the research (Project  
12 ID: 12030202). This study was partially funded by the National Key R&D Program of China  
13 (No. 2017YFE0114300)

14  
15  
16  
17  
18  
19  
20  
21  
22  
**References**

- 23  
24  
25  
26 [1] R. Miranda, C. Negro, A. Blanco, Internal treatment of process waters in paper production  
27 by dissolved air flotation with newly developed chemicals. 1. Laboratory tests, Ind. Eng.  
28 Chem. Res. 48 (2009) 2199–2205. <https://doi.org/10.1021/ie801047h>.
- 29  
30  
31 [2] A.C. Rodrigues, M. Boroski, N.S. Shimada, J.C. Garcia, J. Nozaki, N. Hioka, Treatment  
32 of paper pulp and paper mill wastewater by coagulation-flocculation followed by  
33 heterogeneous photocatalysis, J. Photochem. Photobiol. A Chem. 194 (2008) 1–10.  
34 https://doi.org/10.1016/j.jphotochem.2007.07.007.
- 35  
36  
37 [3] A.A. Sari, U. Hanifah, Y. Parmawati, R. Permadi, Development of immobilized activated  
38 carbon-enzyme for decolorization of black liquor, Key Eng. Mater. 775 KEM (2018) 402–  
39 407. <https://doi.org/10.4028/www.scientific.net/KEM.775.402>.
- 40  
41  
42 [4] M. Ksibi, S. Ben Amor, S. Cherif, E. Elaloui, A. Houas, M. Elaloui, Photodegradation of  
43 lignin from black liquor using a UV/TiO<sub>2</sub> system, J. Photochem. Photobiol. A Chem. 154  
44 (2003) 211–218. [https://doi.org/10.1016/S1010-6030\(02\)00316-7](https://doi.org/10.1016/S1010-6030(02)00316-7).

- [5] F. Torrades, S. Saiz, J.A. García-Hortal, J. García-Montaño, Degradation of wheat straw black liquor by Fenton and photo-Fenton processes, Environ. Eng. Sci. 25 (2008) 92–98. <https://doi.org/10.1089/ees.2007.0021>.
- [6] N.S. Kevlich, M.L. Shofner, S. Nair, Membranes for Kraft black liquor concentration and chemical recovery: Current progress, challenges, and opportunities, Sep. Sci. Technol. 52 (2017) 1070–1094. <https://doi.org/10.1080/01496395.2017.1279180>.
- [7] C.H. Ko, P.H. Hsieh, M.W. Chang, J.M. Chern, S.M. Chiang, C.J. Tzeng, Kinetics of pulp mill effluent treatment by ozone-based processes, J. Hazard. Mater. 168 (2009) 875–881. <https://doi.org/10.1016/j.jhazmat.2009.02.111>.
- [8] L. Miao, F. Li, J. Wen, Biological treatment of high-pH and high-concentration black liquor of cotton pulp by an immediate aerobic-anaerobic-aerobic process, Water Sci. Technol. 60 (2009) 3275–3284. <https://doi.org/10.2166/wst.2009.737>.
- [9] G. Morales, S. Pesante, G. Vidal, Effects of black liquor shocks on activated sludge treatment of bleached kraft pulp mill wastewater, J. Environ. Sci. Heal. - Part A Toxic/Hazardous Subst. Environ. Eng. 50 (2015) 639–645. <https://doi.org/10.1080/10934529.2015.994974>.
- [10] J. Van Der Waarde, J. Krooneman, B. Geurkink, A. Van Der Werf, D. Eikelboom, C. Beimfohr, J. Snaidr, C. Levantesi, V. Tandoi, Molecular monitoring of bulking sludge in industrial wastewater treatment plants, Water Sci. Technol. 46 (2002) 551–558. <https://doi.org/10.2166/wst.2002.0533>.
- [11] S. Kortekaas, J.I.M.A. Field, Anaerobic-Aerobic Treatment of Toxic Pulping Black

1  
2  
3  
4 Liquor with Upfront Effluent Recirculation, 86 (1998) 97–110.  
5  
6

- 7 [12] H. Roy Ghatak, Electrolysis of black liquor for hydrogen production: Some initial  
8 findings, Int. J. Hydrogen Energy. 31 (2006) 934–938.  
9  
10 https://doi.org/10.1016/j.ijhydene.2005.07.013.  
11  
12 [13] G. Nong, Z. Zhou, S. Wang, Generation of hydrogen, lignin and sodium hydroxide from  
13 pulping black liquor by electrolysis, Energies. 9 (2016).  
14  
15 https://doi.org/10.3390/en9010013.  
16  
17 [14] A. Darmawan, M.W. Ajiwibowo, M.K. Biddinika, K. Tokimatsu, M. Aziz, Black liquor-  
18 based hydrogen and power co-production: Combination of supercritical water gasification  
19 and syngas chemical looping, Appl. Energy. 252 (2019) 113446.  
20  
21 https://doi.org/10.1016/j.apenergy.2019.113446.  
22  
23  
24 [15] E. Andersson, S. Harvey, System analysis of hydrogen production from gasified black  
25 liquor, Energy. 31 (2006) 3426–3434. https://doi.org/10.1016/j.energy.2006.03.015.  
26  
27  
28 [16] E. Vaez, M. Taherdanak, H. Zilouei, Dark Hydrogen Fermentation From Paper Mill  
29 Effluent ( PME ): The influence of Substrate Concentration and Hydrolysis, Environ.  
30 Energy Econ. Res. 1 (2017) 163–170. https://doi.org/10.22097/eeer.2017.47243.  
31  
32  
33 [17] A. Elreedy, E. Ibrahim, N. Hassan, A. El-Dissouky, M. Fujii, C. Yoshimura, A. Tawfik,  
34 Nickel-graphene nanocomposite as a novel supplement for enhancement of biohydrogen  
35 production from industrial wastewater containing mono-ethylene glycol, Energy Convers.  
36 Manag. 140 (2017). https://doi.org/10.1016/j.enconman.2017.02.080.  
37  
38  
39 [18] A. Elreedy, M. Fujii, M. Koyama, K. Nakasaki, A. Tawfik, Enhanced fermentative  
40  
41  
42  
43  
44  
45  
46  
47  
48  
49  
50  
51  
52  
53  
54  
55  
56  
57  
58  
59  
60  
61  
62  
63  
64  
65

1  
2  
3  
4 hydrogen production from industrial wastewater using mixed culture bacteria incorporated  
5 with iron, nickel, and zinc-based nanoparticles, Water Res. 151 (2019) 349–361.  
6  
7 https://doi.org/10.1016/j.watres.2018.12.043.

8  
9  
10 [19] A.H. Salem, T. Mietzel, R. Brunstermann, R. Widmann, Effect of cell immobilization,  
11 hematite nanoparticles and formation of hydrogen-producing granules on biohydrogen  
12 production from sucrose wastewater, Int. J. Hydrogen Energy. 42 (2017) 25225–25233.  
13  
14 https://doi.org/10.1016/j.ijhydene.2017.08.060.

15  
16 [20] A. Mostafa, A. El-Dissouky, A. Fawzy, A. Farghaly, P. Peu, P. Dabert, S. Le Roux, A.  
17 Tawfik, Magnetite/graphene oxide nano-composite for enhancement of hydrogen  
18 production from gelatinaceous wastewater, Bioresour. Technol. 216 (2016).  
19  
20 https://doi.org/10.1016/j.biortech.2016.05.072.

21  
22 [21] T. Jayabalan, M. Manickam, S. Naina Mohamed, NiCo<sub>2</sub>O<sub>4</sub>-graphene nanocomposites in  
23 sugar industry wastewater fed microbial electrolysis cell for enhanced biohydrogen  
24 production, Renew. Energy. 154 (2020) 1144–1152.  
25  
26 https://doi.org/10.1016/j.renene.2020.03.071.

27  
28 [22] M.A. Hassan, A.M. Mohammad, T.A. Salaheldin, B.E. El-Anadouli, A promising  
29 hydroxyapatite/graphene hybrid nanocomposite for methylene blue dye's removal in  
30 wastewater treatment, Int. J. Electrochem. Sci. 13 (2018) 8222–8240.  
31  
32 https://doi.org/10.20964/2018.08.77.

33  
34 [23] P. Kahrizi, F.S. Mohseni-Shahri, F. Moeinpour, Adsorptive removal of cadmium from  
35 aqueous solutions using NiFe<sub>2</sub>O<sub>4</sub>/hydroxyapatite/graphene quantum dots as a novel nano-  
36 adsorbent, J. Nanostructure Chem. 8 (2018) 441–452. https://doi.org/10.1007/s40097-018-  
37  
38  
39  
40  
41  
42  
43  
44  
45  
46  
47  
48  
49  
50  
51  
52  
53  
54  
55  
56  
57  
58  
59  
60  
61  
62  
63  
64  
65

1  
2  
3  
4  
5  
6  
7  
8 0284-3.  
9  
10  
11  
12  
13  
14  
15  
16  
17  
18  
19  
20  
21  
22  
23  
24  
25  
26  
27  
28  
29  
30  
31  
32  
33  
34  
35  
36  
37  
38  
39  
40  
41  
42  
43  
44  
45  
46  
47  
48  
49  
50  
51  
52  
53  
54  
55  
56  
57  
58  
59  
60  
61  
62  
63  
64  
65

- [24] P. Turon, L.J. del Valle, C. Alemán, J. Puiggalí, Biodegradable and biocompatible systems based on hydroxyapatite nanoparticles, *Appl. Sci.* 7 (2017). <https://doi.org/10.3390/app7010060>.
- [25] T. Wen, X. Wu, M. Liu, Z. Xing, X. Wang, A.W. Xu, Efficient capture of strontium from aqueous solutions using graphene oxide-hydroxyapatite nanocomposites, *Dalt. Trans.* 43 (2014) 7464–7472. <https://doi.org/10.1039/c3dt53591f>.
- [26] G. Bharath, N. Ponpandian, Hydroxyapatite nanoparticles on dendritic  $\alpha$ -Fe<sub>2</sub>O<sub>3</sub> hierarchical architectures for a heterogeneous photocatalyst and adsorption of Pb(II) ions from industrial wastewater, *RSC Adv.* 5 (2015) 84685–84693. <https://doi.org/10.1039/c5ra15703j>.
- [27] F. Safatian, Z. Doago, M. Torabbeigi, H. Rahmani Shams, N. Ahadi, Lead ion removal from water by hydroxyapatite nanostructures synthesized from egg shells with microwave irradiation, *Appl. Water Sci.* 9 (2019) 1–6. <https://doi.org/10.1007/s13201-019-0979-8>.
- [28] J. Chen, B. Yao, C. Li, G. Shi, An improved Hummers method for eco-friendly synthesis of graphene oxide, *Carbon N. Y.* 64 (2013) 225–229. <https://doi.org/10.1016/j.carbon.2013.07.055>.
- [29] R.M. Campbell, N.M. Anderson, D.E. Daugaard, H.T. Naughton, Financial viability of biofuel and biochar production from forest biomass in the face of market price volatility and uncertainty, *Appl. Energy.* 230 (2018) 330–343. <https://doi.org/10.1016/j.apenergy.2018.08.085>.

- [30] K.R.J. Perera, B. Ketheesan, V. Gadhamshetty, N. Nirmalakhandan, Fermentative biohydrogen production: Evaluation of net energy gain, *Int. J. Hydrogen Energy.* 35 (2010) 12224–12233. <https://doi.org/10.1016/j.ijhydene.2010.08.037>.
- [31] Y. Huang, M. Anderson, D. McIlveen-Wright, G.A. Lyons, W.C. McRoberts, Y.D. Wang, A.P. Roskilly, N.J. Hewitt, Biochar and renewable energy generation from poultry litter waste: A technical and economic analysis based on computational simulations, *Appl. Energy.* 160 (2015) 656–663. <https://doi.org/10.1016/j.apenergy.2015.01.029>.
- [32] APHA, *Standard Methods for the Examination of Water and Wastewater*, 25th Ed. Washington, DC Am. Public Heal. Assoc. Water Work. Assoc. Water Environ. Fed. (2005).
- [33] G.L. Miller, Use of Dinitrosalicylic Acid Reagent for Determination of Reducing Sugar, *Anal. Chem.* 31 (1959) 426–428. <https://doi.org/10.1021/ac60147a030>.
- [34] Y.S. Velioglu, G. Mazza, L. Gao, B.D. Oomah, Antioxidant Activity and Total Phenolics in Selected Fruits, Vegetables, and Grain Products, *J. Agric. Food Chem.* 46 (1998) 4113–4117. <https://doi.org/10.1021/jf9801973>.
- [35] A. ROBERTA RE, NICOLETTA PELLEGRINI, ANNA PROTEGGENTE, ANANTH PANNALA, MIN YANG, C. RICE-EVANS, ANTIOXIDANT ACTIVITY APPLYING AN IMPROVED ABTS RADICAL CATION DECOLORIZATION ASSAY, *Free Radic. Biol. Med.* Vol. 26 (1999) 1231–1237.
- [36] M. DuBois, K. a. Gilles, J.K. Hamilton, P. a. Rebers, F. Smith, Colorimetric method for determination of sugars and related substances, *Anal. Chem.* 28 (1956) 350–356.

1  
2  
3  
4 https://doi.org/10.1021/ac60111a017.  
5  
6

7 [37] D. Lee, Y. Li, Y. Oh, M. Kim, T. Noike, Effect of iron concentration on continuous H 2  
8 production using membrane bioreactor, Int. J. Hydrogen Energy. 34 (2009) 1244–1252.  
9  
10  
11

12 https://doi.org/10.1016/j.ijhydene.2008.11.093.  
13  
14

15 [38] Z. Emami Bistgani, S.A. Siadat, A. Bakhshandeh, A. Ghasemi Pirbalouti, M. Hashemi,  
16 Interactive effects of drought stress and chitosan application on physiological  
17 characteristics and essential oil yield of Thymus daenensis Celak, Crop J. 5 (2017) 407–  
18 415. https://doi.org/10.1016/j.cj.2017.04.003.  
19  
20  
21  
22  
23  
24

25 [39] C. Delbès, R. Moletta, J.J. Godon, Bacterial and archaeal 16S rDNA and 16S rRNA  
26 dynamics during an acetate crisis in an anaerobic digestor ecosystem, FEMS Microbiol.  
27 Ecol. 35 (2001) 19–26. https://doi.org/10.1016/S0168-6496(00)00107-0.  
28  
29  
30  
31  
32

33 [40] S. Poirier, E. Desmond-Le Quéméner, C. Madigou, T. Bouchez, O. Chapleur, Anaerobic  
34 digestion of biowaste under extreme ammonia concentration: Identification of key  
35 microbial phylotypes, Bioresour. Technol. 207 (2016) 92–101.  
36  
37 https://doi.org/10.1016/j.biortech.2016.01.124.  
38  
39  
40  
41  
42  
43  
44

45 [41] H. Wu, R.A. Irizarry, H.C. Bravo, Intensity normalization improves color calling in  
46 SOLiD sequencing, Nat. Methods. 7 (2010) 336–337. https://doi.org/10.1038/nmeth0510-  
47 336.  
48  
49  
50  
51  
52

53 [42] P.D. Schloss, S.L. Westcott, T. Ryabin, J.R. Hall, M. Hartmann, E.B. Hollister, R.A.  
54 Lesniewski, B.B. Oakley, D.H. Parks, C.J. Robinson, J.W. Sahl, B. Stres, G.G. Thallinger,  
55 D.J. Van Horn, C.F. Weber, Introducing mothur: Open-source, platform-independent,  
56  
57  
58  
59  
60  
61  
62  
63  
64  
65

1  
2  
3  
4 community-supported software for describing and comparing microbial communities,  
5  
6 Appl. Environ. Microbiol. 75 (2009) 7537–7541. <https://doi.org/10.1128/AEM.01541-09>.  
7  
8  
9

10 [43] R.C. Edgar, UPARSE: Highly accurate OTU sequences from microbial amplicon reads,  
11  
12 Nat. Methods. 10 (2013) 996–998. <https://doi.org/10.1038/nmeth.2604>.  
13  
14  
15

16 [44] R.C. Edgar, Search and clustering orders of magnitude faster than BLAST,  
17  
18 Bioinformatics. 26 (2010) 2460–2461. <https://doi.org/10.1093/bioinformatics/btq461>.  
19  
20

21 [45] H. Oksanen, J., Blanchet, F., Kindt, R., Legendre, P., O'hara, R., Simpson, G., Solymos,  
22  
23 P., Stevens, M. and Wagner, vegan: Community Ecology Package. R package version  
24  
25 1.17-12. R Foundation for Statistical Computing, Vienna, Austria, (2011).  
26  
27  
28

29 [46] M. Bastian, M., Heymann, S. and Jacomy, Gephi: an open source software for exploring  
30  
31 and manipulating networks., (2009).  
32  
33  
34

35 [47] 1 Paul Shannon, 1 Andrew Markiel, 2 Owen Ozier, 2 Nitin S. Baliga, 1 Jonathan T. Wang,  
36  
37 2 Daniel Ramage, 2 Nada Amin, 5 Benno Schwikowski, 1, 5 and Trey Ideker2, 3, 4, 山本  
38 隆久, 豊田直平, 深瀬吉邦, 大森敏行, Cytoscape: A Software Environment for  
39  
40 Integrated Models, Genome Res. 13 (1971) 426.  
41  
42  
43  
44  
45  
46  
47

48 [48] F. Cumbo, P. Paci, D. Santoni, L. Di Paola, A. Giuliani, GIANT: A cytoscape plugin for  
49  
50 modular networks, PLoS One. 9 (2014) 1–7.  
51  
52  
53  
54 https://doi.org/10.1371/journal.pone.0105001.  
55  
56

57 [49] J.M. Olesen, J. Bascompte, Y.L. Dupont, P. Jordano, VR\_Teenart177.pdf, (2007).  
58  
59  
60 https://doi.org/10.1073/pnas.0706375104.  
61  
62  
63  
64  
65

- [50] H. Han, M. Cui, L. Wei, H. Yang, J. Shen, Enhancement effect of hematite nanoparticles on fermentative hydrogen production, *Bioresour. Technol.* 102 (2011) 7903–7909.  
<https://doi.org/10.1016/j.biortech.2011.05.089>.
- [51] G.Z. Kyzas, N.A. Travlou, O. Kalogirou, E.A. Deliyanni, Magnetic graphene oxide: Effect of preparation route on reactive black 5 adsorption, *Materials (Basel)*. 6 (2013) 1360–1376. <https://doi.org/10.3390/ma6041360>.
- [52] L. Nalbandian, E. Patrikiadou, V. Zaspalis, A. Patrikidou, E. Hatzidaki, C. N. Papandreu, Magnetic Nanoparticles in Medical Diagnostic Applications: Synthesis, Characterization and Proteins Conjugation, *Curr. Nanosci.* 12 (2015) 455–468.  
<https://doi.org/10.2174/1573413712666151210230002>.
- [53] B. Cengiz, Y. Gokce, N. Yildiz, Z. Aktas, A. Calimli, Synthesis and characterization of hydroxyapatite nanoparticles, *Colloids Surfaces A Physicochem. Eng. Asp.* 322 (2008) 29–33. <https://doi.org/10.1016/j.colsurfa.2008.02.011>.
- [54] M.T.K. Al-Jabri, M.G. Devi, M. Al Abri, Synthesis, characterization and application of magnetic nanoparticles in the removal of copper from aqueous solution, *Appl. Water Sci.* 8 (2018) 1–7. <https://doi.org/10.1007/s13201-018-0872-x>.
- [55] D.H. Kim, S.H. Kim, H.W. Kim, M.S. Kim, H.S. Shin, Sewage sludge addition to food waste synergistically enhances hydrogen fermentation performance, *Bioresour. Technol.* 102 (2011) 8501–8506. <https://doi.org/10.1016/j.biortech.2011.04.089>.
- [56] F.Y. Chang, C.Y. Lin, Calcium effect on fermentative hydrogen production in an anaerobic up-flow sludge blanket system, *Water Sci. Technol.* 54 (2006) 105–112.

1  
2  
3  
4 https://doi.org/10.2166/wst.2006.867.  
5  
6

7 [57] M. Nasr, A. Tawfik, S. Ookawara, M. Suzuki, S. Kumari, F. Bux, Continuous  
8 biohydrogen production from starch wastewater via sequential dark-photo fermentation  
9 with emphasize on maghemite nanoparticles, J. Ind. Eng. Chem. 21 (2015).  
10  
11

12 https://doi.org/10.1016/j.jiec.2014.03.011.  
13  
14

15 [58] W. Zhao, J. Zhao, G. Chen, R. Feng, J. Yang, Y. Zhao, Q. Wei, B. Du, Y. Zhang,  
16 Anaerobic biohydrogen production by the mixed culture with mesoporous Fe<sub>3</sub>O<sub>4</sub>  
17 nanoparticles activation, Adv. Mater. Res. 306–307 (2011) 1528–1531.  
18  
19

20 https://doi.org/10.4028/www.scientific.net/AMR.306-307.1528.  
21  
22

23 [59] S.N. Malik, V. Pugalenthhi, A.N. Vaidya, P.C. Ghosh, S.N. Mudliar, Kinetics of nano-  
24 catalysed dark fermentative hydrogen production from distillery wastewater, Energy  
25 Procedia. 54 (2014) 417–430. https://doi.org/10.1016/j.egypro.2014.07.284.  
26  
27

28 [60] L. Zhang, L. Zhang, D. Li, Enhanced dark fermentative hydrogen production by zero-  
29 valent iron activated carbon micro-electrolysis, Int. J. Hydrogen Energy. 40 (2015)  
30 12201–12208. https://doi.org/10.1016/j.ijhydene.2015.07.106.  
31  
32

33 [61] N. Kosaric, R. Blaszczyk, L. Orphan, Factors influencing formation and maintenance of  
34 granules in anaerobic sludge blanket reactors (UASBR), Water Sci. Technol. 22 (1990)  
35 275–282. https://doi.org/10.2166/wst.1990.0092.  
36  
37

38 [62] Z. Yuan, H. Yang, X. Zhi, J. Shen, Increased performance of continuous stirred tank  
39 reactor with calcium supplementation, Int. J. Hydrogen Energy. 35 (2010) 2622–2626.  
40  
41 https://doi.org/10.1016/j.ijhydene.2009.04.018.  
42  
43

- [63] A. Gadhe, S.S. Sonawane, M.N. Varma, Enhancement effect of hematite and nickel nanoparticles on biohydrogen production from dairy wastewater, *Int. J. Hydrogen Energy.* 40 (2015) 4502–4511. <https://doi.org/10.1016/j.ijhydene.2015.02.046>.
- [64] A. Gadhe, S.S. Sonawane, M.N. Varma, Influence of nickel and hematite nanoparticle powder on the production of biohydrogen from complex distillery wastewater in batch fermentation, *Int. J. Hydrogen Energy.* 40 (2015) 10734–10743. <https://doi.org/10.1016/j.ijhydene.2015.05.198>.
- [65] A. Mshandete, L. Björnsson, A.K. Kivaisi, S.T. Rubindamayugi, B. Mattiasson, Enhancement of anaerobic batch digestion of sisal pulp waste by mesophilic aerobic pre-treatment, *Water Res.* 39 (2005) 1569–1575. <https://doi.org/10.1016/j.watres.2004.11.037>.
- [66] W. Parawira, Enzyme research and applications in biotechnological intensification of biogas production, *Crit. Rev. Biotechnol.* 32 (2012) 172–186. <https://doi.org/10.3109/07388551.2011.595384>.
- [67] Y. Tang, T. Shigematsu, S. Morimura, K. Kida, Microbial community analysis of mesophilic anaerobic protein degradation process using bovine serum albumin (BSA)-fed continuous cultivation, *J. Biosci. Bioeng.* 99 (2005) 150–164. <https://doi.org/10.1263/jbb.99.150>.
- [68] Z. Bagi, N. Ács, B. Bálint, L. Horváth, K. Dobó, K.R. Perei, G. Rákely, K.L. Kovács, Biotechnological intensification of biogas production, *Appl. Microbiol. Biotechnol.* 76 (2007) 473–482. <https://doi.org/10.1007/s00253-007-1009-6>.
- [69] Y. Feng, Y. Zhang, X. Quan, S. Chen, Enhanced anaerobic digestion of waste activated

1  
2  
3  
4 sludge digestion by the addition of zero valent iron, Water Res. 52 (2014) 242–250.  
5  
6  
7 https://doi.org/10.1016/j.watres.2013.10.072.

8  
9  
10 [70] H.J. Roman, J.E. Burgess, B.I. Pletschke, Enzyme treatment to decrease solids and  
11 improve digestion of primary sewage sludge, African J. Biotechnol. 5 (2006) 963–967.  
12  
13 https://doi.org/10.5897/AJB06.154.

14  
15  
16 [71] K. Luo, Q. Yang, X. ming Li, G. jing Yang, Y. Liu, D. bo Wang, W. Zheng, G. ming  
17 Zeng, Hydrolysis kinetics in anaerobic digestion of waste activated sludge enhanced by  $\alpha$ -  
18 amylase, Biochem. Eng. J. 62 (2012) 17–21. https://doi.org/10.1016/j.bej.2011.12.009.

19  
20  
21 [72] H. Yu, Z. Zhu, W. Hu, H. Zhang, Hydrogen production from rice winery wastewater in an  
22 upflow anaerobic reactor by using mixed anaerobic cultures, Int. J. Hydrogen Energy. 27  
23 (2002) 1359–1365. https://doi.org/10.1016/S0360-3199(02)00073-3.

24  
25  
26 [73] J.W. Morgan, L.M. Evison, C.F. Forster, Changes to the microbial ecology in anaerobic  
27 digesters treating ice cream wastewater during start-up, Water Res. 25 (1991) 639–653.  
28  
29 https://doi.org/10.1016/0043-1354(91)90039-S.

30  
31  
32 [74] G. Yang, P. Zhang, G. Zhang, Y. Wang, A. Yang, Degradation properties of protein and  
33 carbohydrate during sludge anaerobic digestion, Bioresour. Technol. 192 (2015) 126–130.  
34  
35 https://doi.org/10.1016/j.biortech.2015.05.076.

36  
37  
38 [75] Z. Yuan, H. Yang, X. Zhi, J. Shen, Enhancement effect of l-cysteine on dark fermentative  
39 hydrogen production, Int. J. Hydrogen Energy. 33 (2008) 6535–6540.  
40  
41 https://doi.org/10.1016/j.ijhydene.2008.07.065.

42  
43  
44 [76] N.S. Engliman, P.M. Abdul, S.Y. Wu, J.M. Jahim, Influence of iron (II) oxide

nanoparticle on biohydrogen production in thermophilic mixed fermentation, Int. J. Hydrogen Energy. 42 (2017) 27482–27493.

<https://doi.org/10.1016/j.ijhydene.2017.05.224>.

- [77] Z. Zeng, Y. Li, R. Yang, C. Liu, X. Hu, S. Luo, E. Gong, J. Ye, The relationship between reducing sugars and phenolic retention of brown rice after enzymatic extrusion, J. Cereal Sci. 74 (2017) 244–249. <https://doi.org/10.1016/j.jcs.2017.02.016>.
- [78] H. El Moudden, Y. El Idrissi, A. El Yadini, H. Harhar, B. Tabyaoui, M. Tabyaoui, Effect of filtration of olive mill wastewater on the phenolic composition and its influence on antioxidant activity, Pharmacologyonline. 2 (2019) 161–176.
- [79] J.E. Hernandez, R.G.J. Edyvean, Inhibition of biogas production and biodegradability by substituted phenolic compounds in anaerobic sludge, J. Hazard. Mater. 160 (2008) 20–28. <https://doi.org/10.1016/j.jhazmat.2008.02.075>.
- [80] A. Chandrasekar, S. Sagadevan, A. Dakshnamoorthy, Synthesis and characterization of nano-hydroxyapatite (n-HAP) using the wet chemical technique, Int. J. Phys. Sci. 8 (2013) 1639–1645. <https://doi.org/10.5897/IJPS2013.3990>.
- [81] S.M. Mbadinga, L.Y. Wang, L. Zhou, J.F. Liu, J.D. Gu, B.Z. Mu, Microbial communities involved in anaerobic degradation of alkanes, Int. Biodeterior. Biodegrad. 65 (2011) 1–13. <https://doi.org/10.1016/j.ibiod.2010.11.009>.
- [82] C. Cravo-laureau, V. Grossi, D. Raphel, R. Matheron, A. Hirschler-réa, Anaerobic n - Alkane Metabolism by a Desulfatibacillus aliphaticivorans Strain CV2803 T, Appl. Environ. Microbiol. 71 (2005) 3458–3467. <https://doi.org/10.1128/AEM.71.7.3458>.

- [83] S. Chatterjee, P. Karlovsky, Removal of the endocrine disrupter butyl benzyl phthalate from the environment, *Appl. Microbiol. Biotechnol.* 87 (2010) 61–73.  
<https://doi.org/10.1007/s00253-010-2570-y>.
- [84] H.N. Gavala, F. Alatriste-Mondragon, R. Iranpour, B.K. Ahring, Biodegradation of phthalate esters during the mesophilic anaerobic digestion of sludge, *Chemosphere*. 52 (2003) 673–682. [https://doi.org/10.1016/S0045-6535\(03\)00126-7](https://doi.org/10.1016/S0045-6535(03)00126-7).
- [85] A. Awasthi, M. Singh, S.K. Soni, R. Singh, A. Kalra, Biodiversity acts as insurance of productivity of bacterial communities under abiotic perturbations, *ISME J.* 8 (2014) 2445–2452. <https://doi.org/10.1038/ismej.2014.91>.
- [86] X. Ma, B. Zhou, A. Budai, A. Jeng, X. Hao, D. Wei, Y. Zhang, D. Rasse, Study of Biochar Properties by Scanning Electron Microscope – Energy Dispersive X-Ray Spectroscopy (SEM-EDX), *Commun. Soil Sci. Plant Anal.* 47 (2016) 593–601.  
<https://doi.org/10.1080/00103624.2016.1146742>.
- [87] A. Shaaban, S.M. Se, N.M.M. Mitan, M.F. Dimin, Characterization of biochar derived from rubber wood sawdust through slow pyrolysis on surface porosities and functional groups, *Procedia Eng.* 68 (2013) 365–371. <https://doi.org/10.1016/j.proeng.2013.12.193>.
- [88] H. Omara, G.M. Abdeelaal, K. Nadaoka, A. Tawfik, Developing empirical formulas for assessing the scour of vertical and inclined piers, *Mar. Georesources Geotechnol.* 38 (2020). <https://doi.org/10.1080/1064119X.2018.1559901>.
- [89] Y. Liu, X. Zhao, J. Li, D. Ma, R. Han, Characterization of bio-char from pyrolysis of wheat straw and its evaluation on methylene blue adsorption, *Desalin. Water Treat.* 46

1  
2  
3  
4 (2012) 115–123. <https://doi.org/10.1080/19443994.2012.677408>.  
5  
6  
7  
8  
9  
10  
11  
12  
13  
14  
15  
16  
17  
18  
19  
20  
21  
22  
23  
24  
25  
26  
27  
28  
29  
30  
31  
32  
33  
34  
35  
36  
37  
38  
39  
40  
41  
42  
43  
44  
45  
46  
47  
48  
49  
50  
51  
52  
53  
54  
55  
56  
57  
58  
59  
60  
61  
62  
63  
64  
65

- [90] M. Soltan, M. Elsamadony, A. Mostafa, H. Awad, A. Tawfik, Harvesting zero waste from co-digested fruit and vegetable peels via integrated fermentation and pyrolysis processes, Environ. Sci. Pollut. Res. 26 (2019). <https://doi.org/10.1007/s11356-019-04647-8>.
- [91] S.A. Opatokun, T. Kan, A. Al Shoaibi, C. Srinivasakannan, V. Strezov, Characterization of Food Waste and Its Digestate as Feedstock for Thermochemical Processing, Energy and Fuels. 30 (2016) 1589–1597. <https://doi.org/10.1021/acs.energyfuels.5b02183>.

## List of tables

**Table 1a** black liquor (Bl) and inoculum sludge (S) characteristics (Values ±Stdv)

| Parameters  | Black Liquor (BL) | Inoculum sludge (S) |
|---|-------------------|---------------------|
| pH-value  | 12.75±2.1         | 7.8±0.2             |
| CODt -g/L   | 22.3±0.6          | 70.75±0.67          |
| CODs - g/L  | 21.88±0.45        | 3.68±0.03           |
| CODp - g/L  | 0.42±0.05         | 67.07±0.06          |
| CODs/CODt ratio   | 0.98              | 0.05                |
| CODp/CODt ratio   | 0.02              | 0.95                |
| TOC - g/L   | 8.26±0.23         | 26.20±0.13          |
| Total solids (TS) - g/L   | 43.8±0.23         | 132.04±0.34         |
| Volatile solids (VS) - g/L  | 21.85±0.56        | 72.75±0.35          |
| VS/TS ratio   | 0.50              | 0.55                |
| Total phosphorous (TP) - g/L  | 5.79±0.30         | 2.11±0.08           |
| C/P ratio   | 3.85              | 33.53               |
| TKJ-N - g/L   | 1.82±0.09         | 5.32±0.15           |
| C/N ratio   | 12.25             | 13.30               |
| Protein - g/L   | 11.36±0.46        | 33.2±1.9            |
| Carbohydrates- g/L  | 43.5±12.7         | 52.2±0.9            |
| Total reducing sugars (TRS) - mg/L  | 262.8±11.9        | 0.1±0.001           |
| Total phenolic compounds (TPC) - mg/L   | 1718±12.4         | -                   |
| TRS/TPC ratio   | 0.15              | -                   |
| Valerate (HVa)- mg/L  | 2234±56.9         | 22±2.9              |
| Iso-butrate (HBu)- mg/L   | ND*               | ND*                 |
| Propionate (HPr) - mg/L   | ND*               | ND*                 |
| Formate (HFo) - mg/L  | 2033±112          | ND*                 |
| Acetate (HAc) - mg/L  | ND*               | ND*                 |
| The half maximal inhibitory concentration (IC <sub>50</sub> ) (µg Gallic acid equivalent/ mL) | 48.4±0.3          | 1.1±0.08            |
| Antioxidant activity -ABTS (scavenging %)   | 31.9±2.9          | -                   |
| α-amylase- U/100 mL   | ND*               | 9.0±0.4             |
| α- xylanase (used breach xylan)- U/100 mL   | ND*               | 400±7.8             |
| α- xylanase (used birch xylan)- U/100 mL  | ND*               | 15±1.2              |
| CM-cellulase (used filter paper)- U/100 mL  | ND*               | ND*                 |
| CM-cellulase (CM-cellulose)- U/100 mL   | ND*               | 4.1±0.7             |
| Polygalacturonase- U/100 mL   | ND*               | ND*                 |
| Peroxidase- U/100 mL  | ND*               | ND*                 |
| Protease - U/100 mL   | ND*               | 165±6.9             |
| Crystallinity index (%)   | 29.5              | -                   |

ND\*: not detected

**Table 1b** energy dispersive X-Ray (EDX) analysis of the black liquor and inoculum sludge

| Elements                 | Black Liquor (BL) |          |          |         | Inoculum sludge |          |          |         |
|--------------------------|-------------------|----------|----------|---------|-----------------|----------|----------|---------|
|                          | Weight %          | Atomic % | Net Int. | Error % | Weight %        | Atomic % | Net Int. | Error % |
| Carbon (C)               | 21.06             | 29.44    | 19.57    | 13.6    | 44.39           | 55.91    | 51.56    | 10.93   |
| Oxygen (O <sub>2</sub> ) | 44.82             | 47.03    | 110.99   | 9.93    | 30.96           | 29.28    | 42.1     | 12.9    |
| Sodium (Na)              | 26.59             | 19.42    | 118.88   | 8.84    | 2.59            | 1.71     | 11.76    | 15.24   |
| Silica (Si)              | 5.2               | 3.11     | 45.78    | 8.99    | 1.82            | 0.98     | 21.37    | 10.75   |
| Potassium (K)            | 2.32              | 1.0      | 17.25    | 13.35   | 0.58            | 0.22     | 4.9      | 29.4    |
| Nitrogen (N)             |                   |          |          |         | 5.12            | 5.53     | 2        | 37.2    |
| Magnesium (Mg)           |                   |          |          |         | 1.04            | 0.64     | 8.42     | 20.18   |
| Aluminum (AL)            |                   |          |          |         | 1.12            | 0.63     | 11.24    | 15.55   |
| Phosphorous (P)          |                   |          |          |         | 3.19            | 1.56     | 32.64    | 8.52    |
| Sulfur (S)               |                   |          |          |         | 2.36            | 1.11     | 25.15    | 10.96   |
| Chlorine (Cl)            |                   |          |          |         | 0.95            | 0.41     | 9.29     | 18.36   |
| Calcium (Ca)             |                   |          |          |         | 4.1             | 1.5      | 29.1     | 9.1     |
| Iron (Fe)                |                   |          |          |         | 1.8             | 0.5      | 5.9      | 24.3    |

**Table 1c** energy dispersive X-ray (EDX) analysis of the solely and dual nanoparticles

| Nanoparticle                     | Element     | Weight % | Atomic % | Net Int. | Error % |
|----------------------------------|-------------|----------|----------|----------|---------|
| Graphene (nG)                    | Carbon      | 70.4     | 76.01    | 99.85    | 5.83    |
|                                  | Oxygen      | 29.6     | 23.99    | 19.21    | 14.51   |
| Graphene oxide (nGO)             | Carbon      | 54.43    | 61.95    | 62.78    | 8.58    |
|                                  | Oxygen      | 43.52    | 37.18    | 40.94    | 12.71   |
|                                  | Sulfur      | 2.05     | 0.88     | 13.58    | 12.9    |
| Magnetite (nM)                   | Oxygen      | 30.56    | 60.57    | 130.98   | 7.34    |
|                                  | Iron        | 69.44    | 39.43    | 201.84   | 3.08    |
| Hydroxyapatite (NHap)            | Oxygen      | 42.16    | 62.48    | 34.49    | 13.49   |
|                                  | Phosphorous | 18.93    | 14.49    | 135.51   | 4.57    |
|                                  | Calcium     | 38.92    | 23.03    | 189.83   | 3.12    |
| Graphene/hydroxyapatite (nG/Hap) | Carbon      | 28.48    | 42.49    | 23.75    | 12.62   |
|                                  | Oxygen      | 35.73    | 40.02    | 32.15    | 13.6    |
|                                  | Phosphorous | 11.34    | 6.56     | 91.9     | 4.68    |
|                                  | Calcium     | 24.45    | 10.93    | 133.93   | 3.31    |

**Table 2** energy dispersive X-ray (EDX) of sludge (S) +black liquor (BL) +nG/Hap before and after fermentation

| Elements                 | Sludge (S) +black liquor (BL) +nG/Hap<br>before fermentation |          |          |         | sludge (S) and black liquor (BL) + nG/Hap<br>after fermentation |          |          |         |
|--------------------------|--|----------|----------|---------|---|----------|----------|---------|
|                          | Weight %   | Atomic % | Net Int. | Error % | Weight %  | Atomic % | Net Int. | Error % |
| Carbon (C)               | 47.51  | 58.2     | 59.64    | 10.45   | 41.85   | 52.46    | 53.34    | 10.81   |
| Oxygen (O <sub>2</sub> ) | 35.22  | 32.39    | 56.5     | 11.96   | 39.95   | 37.6     | 73.72    | 11.47   |
| Silica (Si)              | 3.04   | 1.59     | 35.42    | 8.12    | 5.03  | 2.7      | 61.47    | 6.74    |
| Potassium (K)            |  |          |          |         | 1   | 0.38     | 8.93     | 17.8    |
| Magnesium (Mg)           |  |          |          |         | 0.82  | 0.51     | 6.87     | 21.15   |
| Aluminum (AL)            | 1.08   | 0.59     | 10.78    | 14.26   | 1.24  | 0.69     | 13.02    | 14      |
| Phosphorous (P)          | 2.22   | 1.05     | 22.22    | 9.98    | 3.1   | 1.51     | 31.93    | 8.62    |
| Sulfur (S)               | 1.74   | 0.8      | 18.38    | 11.6    |   |          |          |         |
| Calcium (Ca)             | 1.87   | 0.69     | 13.55    | 14.08   | 1.53  | 0.58     | 11.67    | 15.94   |

**Table 3** GC-mass analysis of the control sample (S+BL) before and after fermentation as well as the batches containing nGO, nM, nG/Hap

| Compounds  | RT   | S+ BL - before fermentation |      | S+ BL+ nGO -after fermentation |      | S+ BL+ nG/Hap -after fermentation |      | S+ BL+nM -after fermentation |      |
|--|------|-----------------------------|------|--------------------------------|------|-----------------------------------|------|------------------------------|------|
|  |      | Area                        | Area | R%                             | Area | R%                                | Area | R%                           | Area |
| 1H-Cyclopropa[3,4]benz[1,2-e]azulene-5,7b,9,9a-tetrol, 1a,1b,4,4a,5,7a,8,9-octahydro-3-(hydroxymethyl)-1,1,6,8-tetramethyl-, 5,9,9a-triacetate ( $C_{26}H_{36}O_8$ )   | 5.18 | 285684.44                   | ND*  | 100                            | ND*  | 100                               | ND*  | 100                          | ND*  |
| 21-Deoxy-16-methoxy-22 $\beta$ -methyl-4,25-secoobscurinervan ( $C_{23}H_{32}N_2O_2$ )   | 5.18 | 285684.44                   | ND*  | 100                            | ND*  | 100                               | ND*  | 100                          | ND*  |
| 2-Nonadecanone 2,4-dinitrophenylhydrazine ( $C_{25}H_{42}N_4O_4$ )   | 5.18 | 285684.44                   | ND*  | 100                            | ND*  | 100                               | ND*  | 100                          | ND*  |
| DHomo-24-nor-17-oxachola-20,22-diene-3,16-dio  | 5.26 | 821571.41                   | ND*  | 100                            | ND*  | 100                               | ND*  | 100                          | ND*  |
| ne,7-(acetoxy)1,2:14,15:21,23-triepoxy4,4,8-trimethyl, (5 $\alpha$ ,7 $\alpha$ ,13 $\alpha$ ,14 $\alpha$ ,15 $\alpha$ ,17 $\alpha$ ) ( $C_{28}H_{34}O_8$ )   | 5.26 | 821571.41                   | ND*  | 100                            | ND*  | 100                               | ND*  | 100                          | ND*  |
| [(1S,7S,8S,12R,20R)-7-(furan-3-yl)-1,8,12,17,17-pentamethyl-5,16-dioxo-3,6,14-trioxahexacyclo[9.9.0.0 <sup>2,4</sup> .0 <sup>2,8</sup> .0 <sup>12,18</sup> .0 <sup>13,15</sup> ]icosan-20-yl] acetate (EPOXYGEDUNIN) ( $C_{28}H_{34}O_8$ ) | 5.26 | 821571.41                   | ND*  | 100                            | ND*  | 100                               | ND*  | 100                          | ND*  |
| 9-Desoxy-9 $\alpha$ -chloroingol 3,7,8,12-tetraacetate ( $C_{28}H_{39}ClO_9$ )   | 5.26 | 821571.41                   | ND*  | 100                            | ND*  | 100                               | ND*  | 100                          | ND*  |
| Betamethasone acetate ( $C_{24}H_{31}FO_6$ )   | 5.35 | 374026.75                   | ND*  | 100                            | ND*  | 100                               | ND*  | 100                          | ND*  |
| O,NPERMETHYLATED ACMETGLYMETM ET ( $C_{24}H_{44}N_4O_6S_3$ )   | 5.35 | 374026.75                   | ND*  | 100                            | ND*  | 100                               | ND*  | 100                          | ND*  |
| 3,9-Epoxypregn-16-ene-1418-diol-20-one,7,11-diacetoxy-3-methoxy ( $C_{26}H_{36}O_9$ )  | 5.35 | 374026.75                   | ND*  | 100                            | ND*  | 100                               | ND*  | 100                          | ND*  |
| Pregnan-7,8,9,11,20-pentaol-18-oicacid,7,11-diacetate-18,20-lactone ( $C_{25}H_{34}O_9$ )  | 5.41 | 473466.77                   | ND*  | 100                            | ND*  | 100                               | ND*  | 100                          | ND*  |
| 6-HDibenzo[b,d]pyran-1,8diol,3-(1,1-dimethylpentyl)6a,7,8,9,10,10-ahexahydro6,6dimethyl9methylene,[6aR(6a $\alpha$ ,8 $\alpha$ ,10a $\alpha$ )] ( $C_{23}H_{34}O_3$ )  | 5.41 | 473466.77                   | ND*  | 100                            | ND*  | 100                               | ND*  | 100                          | ND*  |
| Bromthymol Blue ( $C_{27}H_{28}Br_2O_5S$ )   | 5.5  | 302510.18                   | ND*  | 100                            | ND*  | 100                               | ND*  | 100                          | ND*  |

|   |           |           |            |            |        |            |        |     |     |            |        |
|---|-----------|-----------|------------|------------|--------|------------|--------|-----|-----|------------|--------|
| PALLADIUMBIS(5-(3,3-DIMETHYL5OXOPYRROLIDIN2YLIDENEMETHYL)3,3-DIMETHYL-2-METHYLENE-3,4-DIHYDRO-2-HPYRROLIUM)   | 5.5       | 302510.18 | ND*        | 100        | ND*    | 100        | ND*    | 100 | ND* | 100        |        |
| COMPLEXn ( $C_{28}H_{38}N_4O_2Pd$ )   |           |           |            |            |        |            |        |     |     |            |        |
| 1[2,4,6tris(trimethylsiloxy)phenyl]3[3,4di(trimethylsiloxy)phenyl]2propen1one C30H52O6Si5   | 5.59      | 515958.25 | ND*        | 100        | ND*    | 100        | ND*    | 100 | ND* | 100        |        |
| Methyl-1-{4-Methoxy-3-chloro-6[2[3(2'-methoxy-5'(1,3-dioxan-2-yl)phenyl)-4-methoxyphenyl]ethyl]phenyl}-2-methoxybenzene-4-carboxylate ( $C_{36}H_{37}ClO_8$ ) | 5.59      | 515958.25 | ND*        | 100        | ND*    | 100        | ND*    | 100 | ND* | 100        |        |
| 5''-(1,1-Dimethylethyl)2,2',2'',2'''-pentamethoxy[1,1':3',1":3",1'''":3'''".1''''''quinquephenyl]3,3'''-dimethanol ( $C_{41}H_{44}O_7$ )                      | 5.59      | 515958.25 | ND*        | 100        | ND*    | 100        | ND*    | 100 | ND* | 100        |        |
| 1b,4a-Epoxy-2H-cyclopenta-[3,4]-cyclopropanoundec[1,2b]oxirens-(1aH)one,2,7,9,10-tetrakis(acetoxy)decahydro3,6,8,8,10-apentamethyl ( $C_{28}H_{38}O_{11}$ )   | [8,9]-cyc | 7.48      | 341117.54  | ND*        | 100    | ND*        | 100    | ND* | 100 | ND*        | 100    |
| ISOCHIAPIN B ( $C_{19}H_{22}O_6$ )  |           | 7.48      | 341117.54  | ND*        | 100    | ND*        | 100    | ND* | 100 | ND*        | 100    |
| 2-Undecanol ( $C_{11}H_{24}O$ )   |           | 19.25     | 381633.05  | ND*        | 100    | ND*        | 100    | ND* | 100 | ND*        | 100    |
| 1-Hexadecene ( $C_{16}H_{32}$ )   |           | 19.25     | 381633.05  | ND*        | 100    | 854127.92  | -123.8 | ND* | 100 | ND*        | 100    |
| 2-Dodecanol ( $C_{12}H_{26}O$ )   |           | 19.25     | 381633.05  | ND*        | 100    | ND*        | 100    | ND* | 100 | ND*        | 100    |
| Docosane ( $C_{22}H_{46}$ )   |           | 21.77     | 670282.78  | ND*        | 100    | 692653.67  | -3.3   | ND* | 100 | ND*        | 100    |
| Pentacosane ( $C_{25}H_{52}$ )  |           | 21.77     | 670282.78  | ND*        | 100    | ND*        | 100    | ND* | 100 | ND*        | 100    |
| Heptadecane ( $C_{17}H_{36}$ )  |           | 21.77     | 670282.78  | ND*        | 100    | ND*        | 100    | ND* | 100 | ND*        | 100    |
| Hexadecane,1,1bis(dodecyloxy) ( $C_{40}H_{82}O_2$ )   |           | 24.01     | 525338.15  | ND*        | 100    | ND*        | 100    | ND* | 100 | ND*        | 100    |
| Tridecanol  |           | 24.01     | 525338.15  | ND*        | 100    | ND*        | 100    | ND* | 100 | ND*        | 100    |
| Docosane ( $C_{22}H_{46}$ )   |           | 25.25     | 625579.51  | ND*        | 100    | 931880.72  | -48.9  | ND* | 100 | 1171229.65 | -87.2  |
| Heptadecane   |           | 25.25     | 625579.51  | ND*        | 100    | ND*        | 100    | ND* | 100 | ND*        | 100    |
| Nonacosane ( $C_{29}H_{60}$ )   |           | 25.25     | 625579.51  | ND*        | 100    | 931880.72  | -48.96 | ND* | 100 | 1171229.65 | -87.2  |
| Dodecane, 2,2,4,9,11,11hexamethyl ( $C_{18}H_{38}$ )  |           | 26.58     | 611364.56  | ND*        | 100    | ND*        | 100    | ND* | 100 | ND*        | 100    |
| Docosane ( $C_{22}H_{46}$ )   |           | 26.58     | 611364.56  | ND*        | 100    | 863160.95  | -41.18 | ND* | 100 | ND*        | 100    |
| Octadecane, 5,14dibutyl ( $C_{26}H_{54}$ )  |           | 26.58     | 611364.56  | ND*        | 100    | ND*        | 100    | ND* | 100 | ND*        | 100    |
| Docosane ( $C_{22}H_{46}$ )   |           | 28.63     | 560055.3   | ND*        | 100    | 1440594.32 | -157.2 | ND* | 100 | ND*        | 100    |
| Nonacosane ( $C_{29}H_{60}$ )   |           | 28.63     | 560055.3   | ND*        | 100    | 1440594.32 | -157.2 | ND* | 100 | 1805397.92 | -222.3 |
| Heptadecane, 9hexyl ( $C_{23}H_{48}$ )  |           | 28.63     | 560055.3   | ND*        | 100    | 1440594.32 | -157.2 | ND* | 100 | ND*        | 100    |
| Isopropyl myristate ( $C_{17}H_{34}O_2$ )   |           | 29.04     | 2174603.97 | 3734650.08 | -71.7  | 7730849.24 | -255.5 | ND* | 100 | 14339279   | -559.3 |
| Tetradecanoic acid ( $C_{14}H_{28}O_2$ )  |           | 29.04     | 2174603.97 | ND*        | 100    | ND*        | 100    | ND* | 100 | ND*        | 100    |
| 4OMethylconhypoprotocetraric acid C19H18O8  |           | 31.85     | 446966.82  | ND*        | 100    | ND*        | 100    | ND* | 100 | ND*        | 100    |
| 1,2-Benzenedicarboxylic acid, dibutyl ester ( $C_{16}H_{22}O_4$ )   |           | 31.85     | 446966.82  | 1032473.15 | -130.9 | 2217406.99 | -      | ND* | 100 | 3924657.98 | -778.0 |
|   |           |           |            |            |        |            | 396.10 |     |     |            |        |
| 1,2-Benzenedicarboxylic acid, butyl octyl ester ( $C_{20}H_{30}O_4$ )   |           | 31.85     | 446966.82  | ND*        | 100    | 2217406.99 | -396.1 | ND* | 100 | ND*        | 100    |
| Cyclodicasiloxane, eicosamethyl ( $C_{20}H_{60}O_{10}Si_{10}$ )   |           | 32.06     | 1132451    | 1646473.49 | -45.3  | 4022466.16 | -255.2 | ND* | 100 | 7219063.77 | -537.4 |
| EICOSAMETHYLCYC   |           | 32.06     | 1132451    | 1646473.49 | -45.3  | 4022466.16 | -255.2 | ND* | 100 | 7219063.77 | -537.4 |

|  |       |           |            |       |            |     |     |     |            |        |  |  |  |
|--|-------|-----------|------------|-------|------------|-----|-----|-----|------------|--------|--|--|--|
| LODECASIOXANE(C <sub>20</sub> H <sub>60</sub> O <sub>10</sub> Si <sub>10</sub> )                       |       |           |            |       |            |     |     |     |            |        |  |  |  |
| 1HPurin6amine, [(2fluorophenyl) methyl](C <sub>12</sub> H <sub>10</sub> FN <sub>5</sub> )              | 32.06 | 1132451   | ND*        | 100   | ND*        | 100 | ND* | 100 | 7219063.77 | -537.4 |  |  |  |
| 1,2-Benzenedicarboxylic acid, mono(2ethylhexyl)ester (C <sub>16</sub> H <sub>22</sub> O <sub>4</sub> ) | 41.62 | 5258093.7 | ND*        | 100   | 16862491.3 | -   | ND* | 100 | ND*        | 100    |  |  |  |
| 1,2-Benzenedicarboxylic acid, dioctyl ester (C <sub>24</sub> H <sub>38</sub> O <sub>4</sub> )          | 41.62 | 5258093.7 | 6386661.04 | -21.4 | 16862491.3 | -   | ND* | 100 | ND*        | 100    |  |  |  |
| 1,2-Benzenedicarboxylic acid, bis(2ethylhexyl) ester (C <sub>24</sub> H <sub>38</sub> O <sub>4</sub> ) | 41.62 | 5258093.7 | 6386661.04 | -21.4 | ND*        | 100 | ND* | 100 | ND*        | 100    |  |  |  |

**Table 4** chemical and textural characteristics for the bio-char

| Element         | Weight % | Atomic % | Net Int. | Error % |
|-----------------|----------|----------|----------|---------|
| Carbon (C )     | 13.73    | 22.5     | 4.23     | 22.08   |
| Oxygen (O)      | 37.44    | 46.07    | 36.64    | 12.37   |
| Sodium (Na)     | 11.98    | 10.26    | 23.41    | 12.91   |
| Magnesium (Mg)  | 0.95     | 0.77     | 2.89     | 63.35   |
| Aluminum (Al)   | 2.32     | 1.7      | 9.11     | 19.35   |
| Silica (Si)     | 9.18     | 6.43     | 43.07    | 8.92    |
| Phosphorous (P) | 6.48     | 4.12     | 25.36    | 11.12   |
| Sulfur (S)      | 2.43     | 1.49     | 10.14    | 18.33   |
| Chlorine (Cl)   | 0.64     | 0.35     | 2.55     | 65.23   |
| Potassium (K)   | 1.72     | 0.87     | 6.39     | 22.88   |

## List of figures

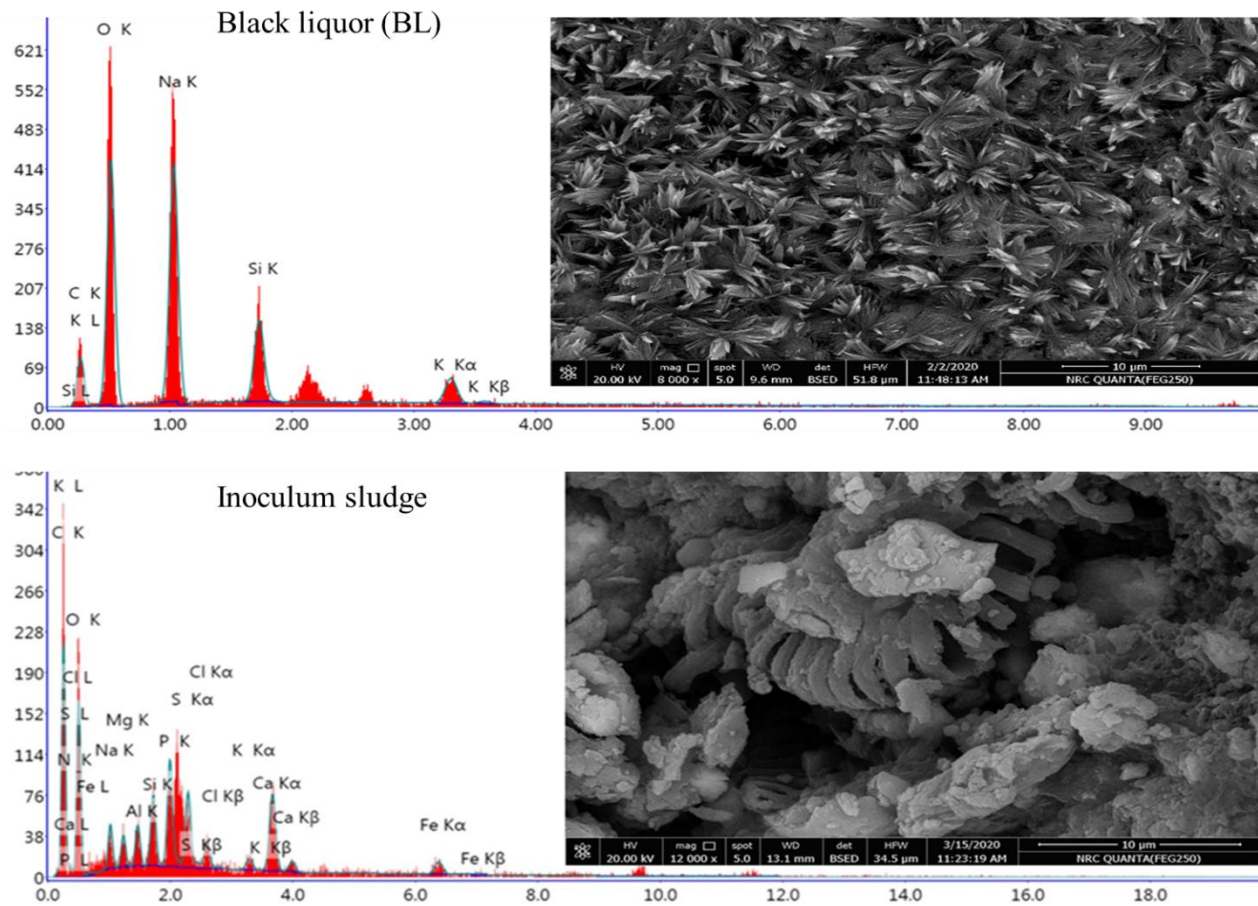


**Fig. 1a** scanning electron microscope (SEM) image and energy dispersive X-Ray (EDX) analysis of the black liquor (BL) and inoculum sludge

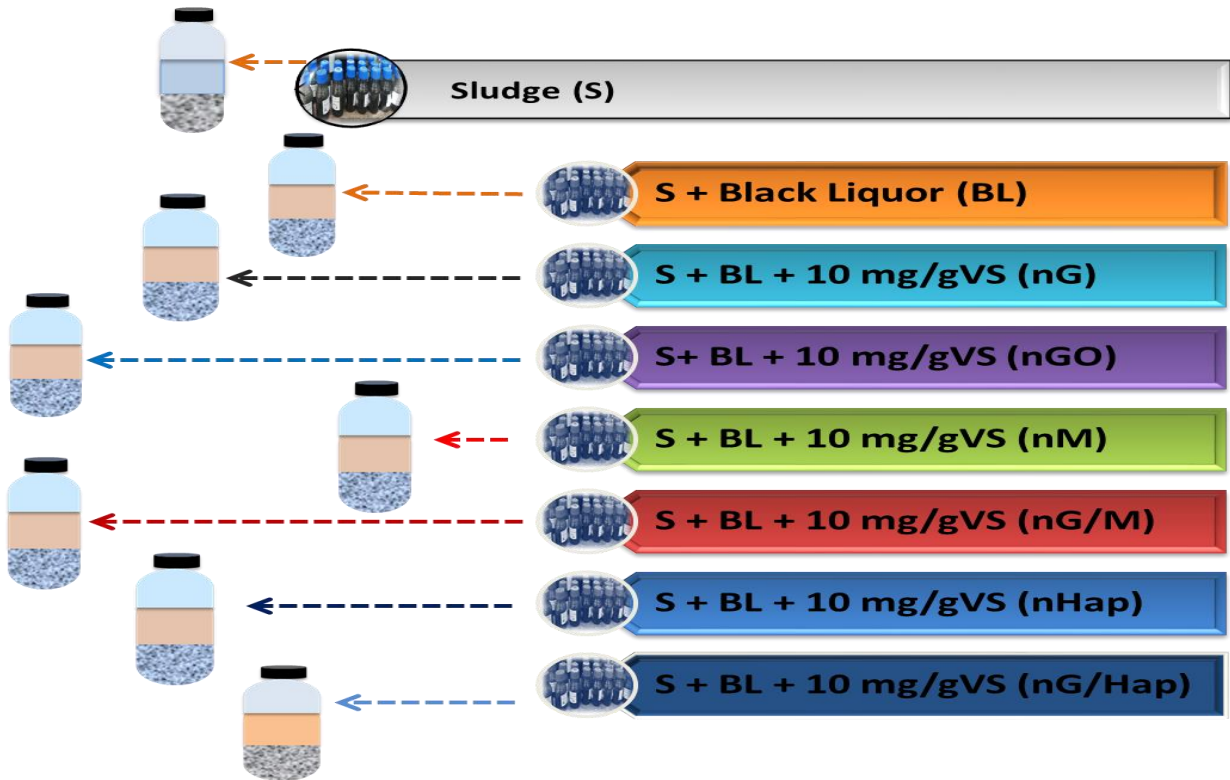


**Fig. 1b** experimental set-up of anaerobic batch assays

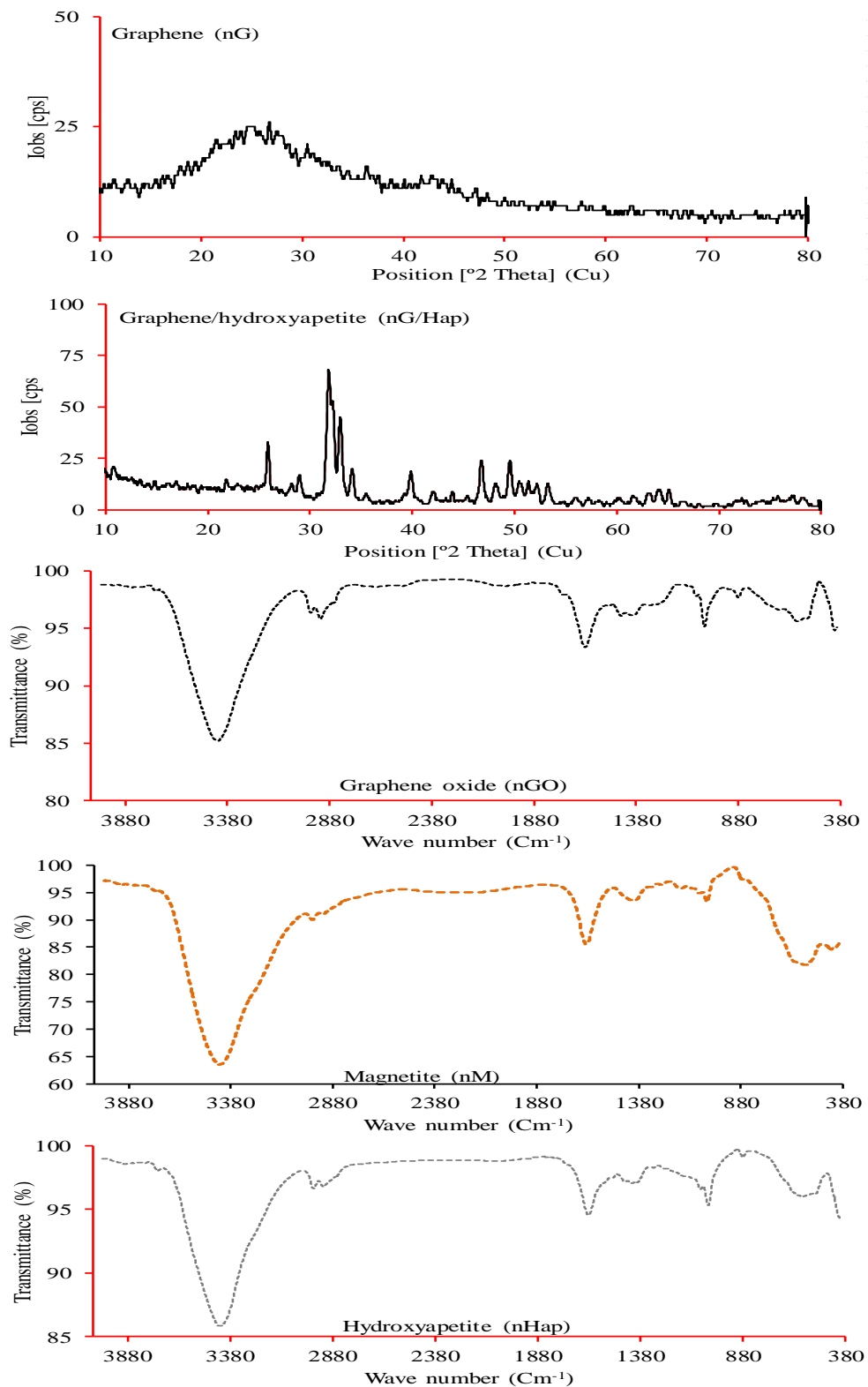


**Fig. 2a** X-ray diffraction (XRD) for Graphene (nG) and Graphene/hydroxyapatite (nG/Hap) & Fourier transform infra-red (FTIR) spectra for graphene oxide (nGO), magnetite (nM) and hydroxyapatite (nHap)

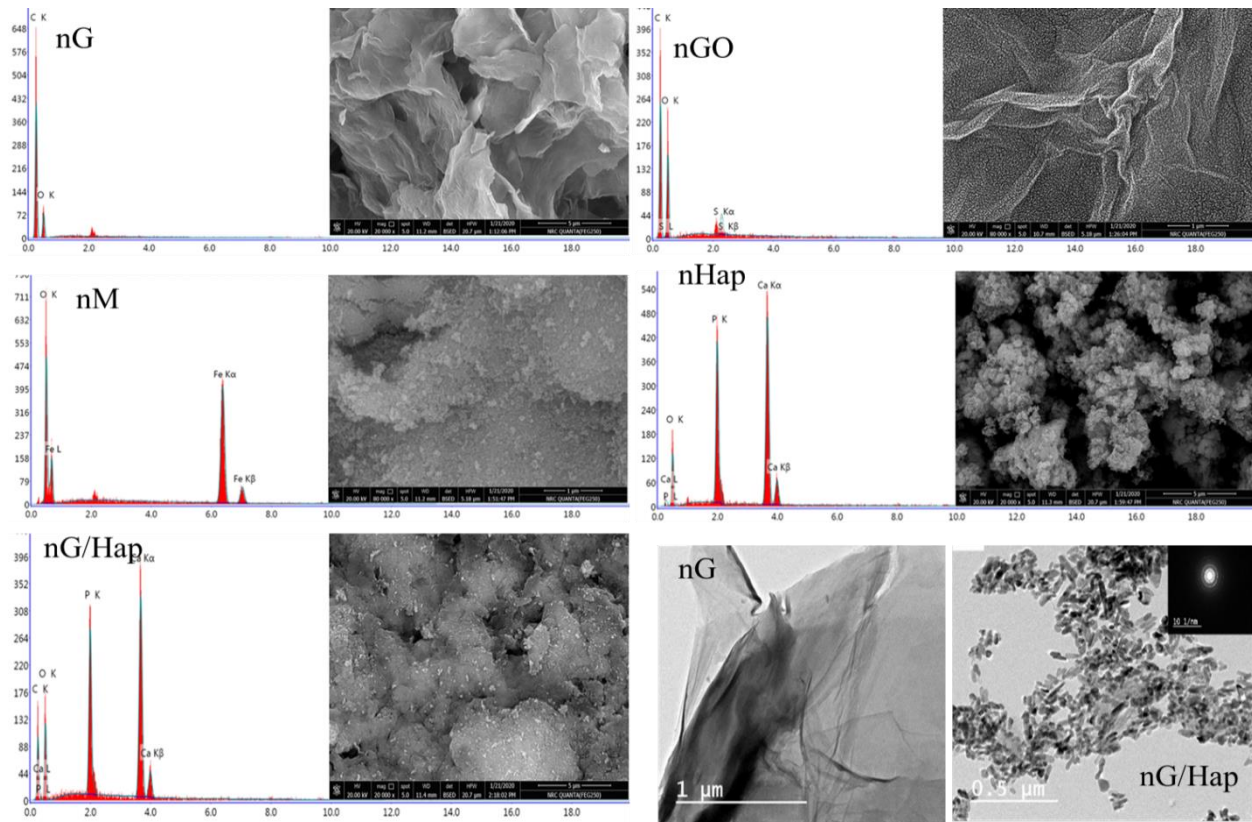


**Fig. 2b** scanning electron microscopy (SEM), and Energy dispersive X-ray (EDX) of graphene (nG), graphene oxide (nGO), magnetite (nM), hydroxyapatite (nHap) and graphene-hydroxyapatite (nG/Hap) and Transmission electron microscopy (TEM) images for graphene (nG) and graphene/hydroxyapatite diffraction (nG/Hap)

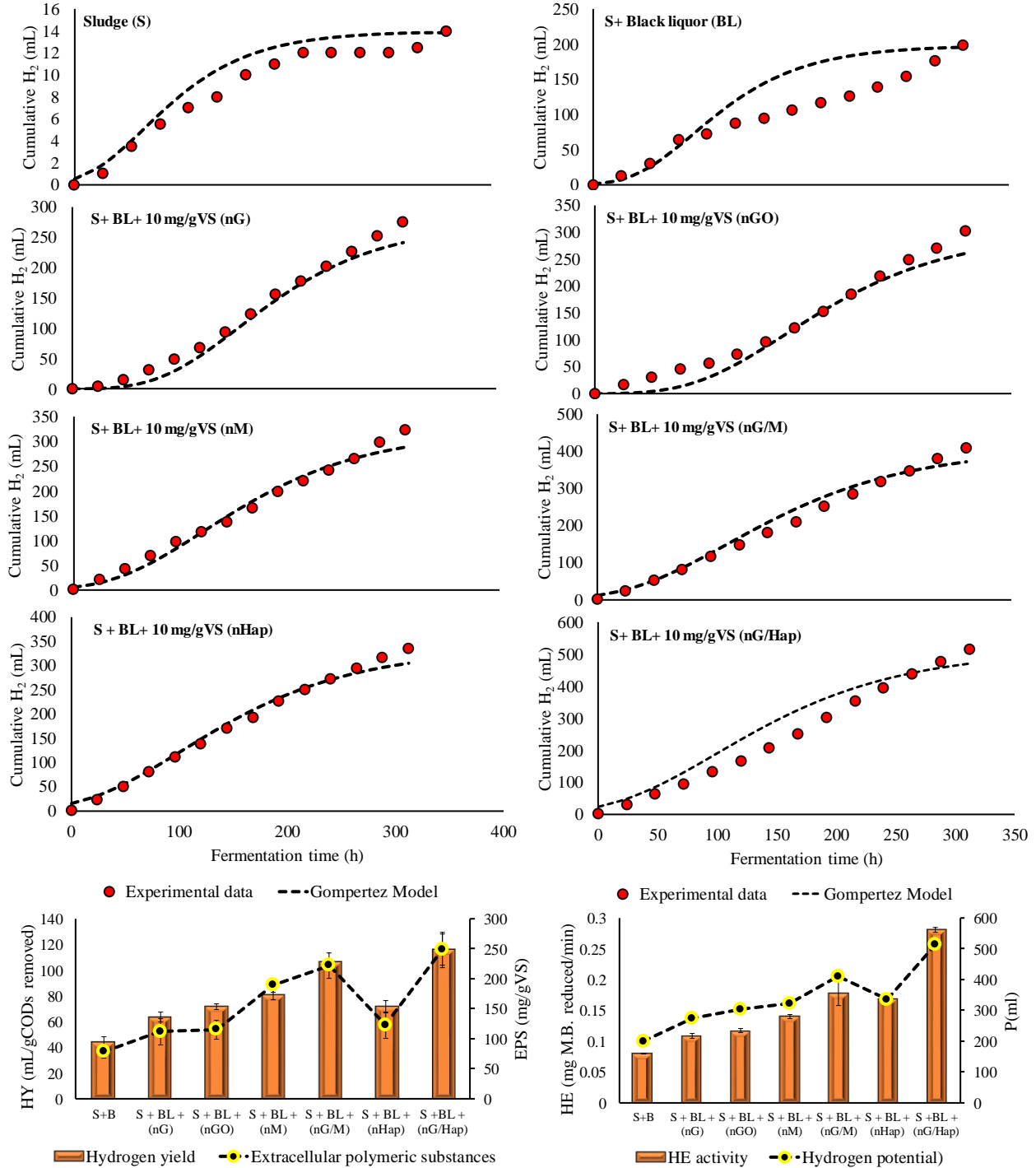


**Fig. 2c** the experimental and modeled data for bio-H<sub>2</sub> production based on modified Gompertz equation, hydrogen yield (HY) versus extracellular polymeric substances (EPS), hydrogenase enzyme (HE) activity versus hydrogen potential (P)

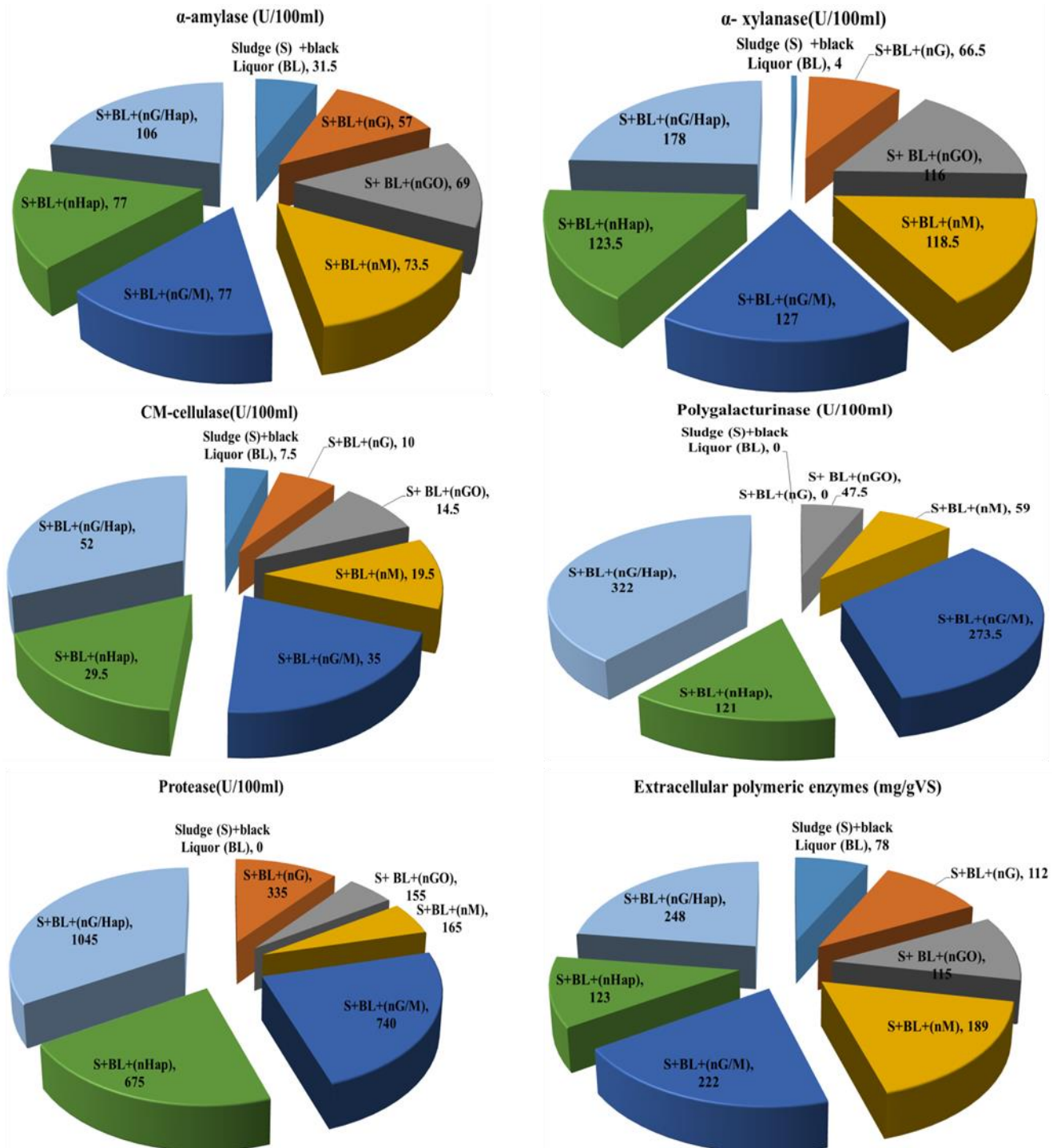
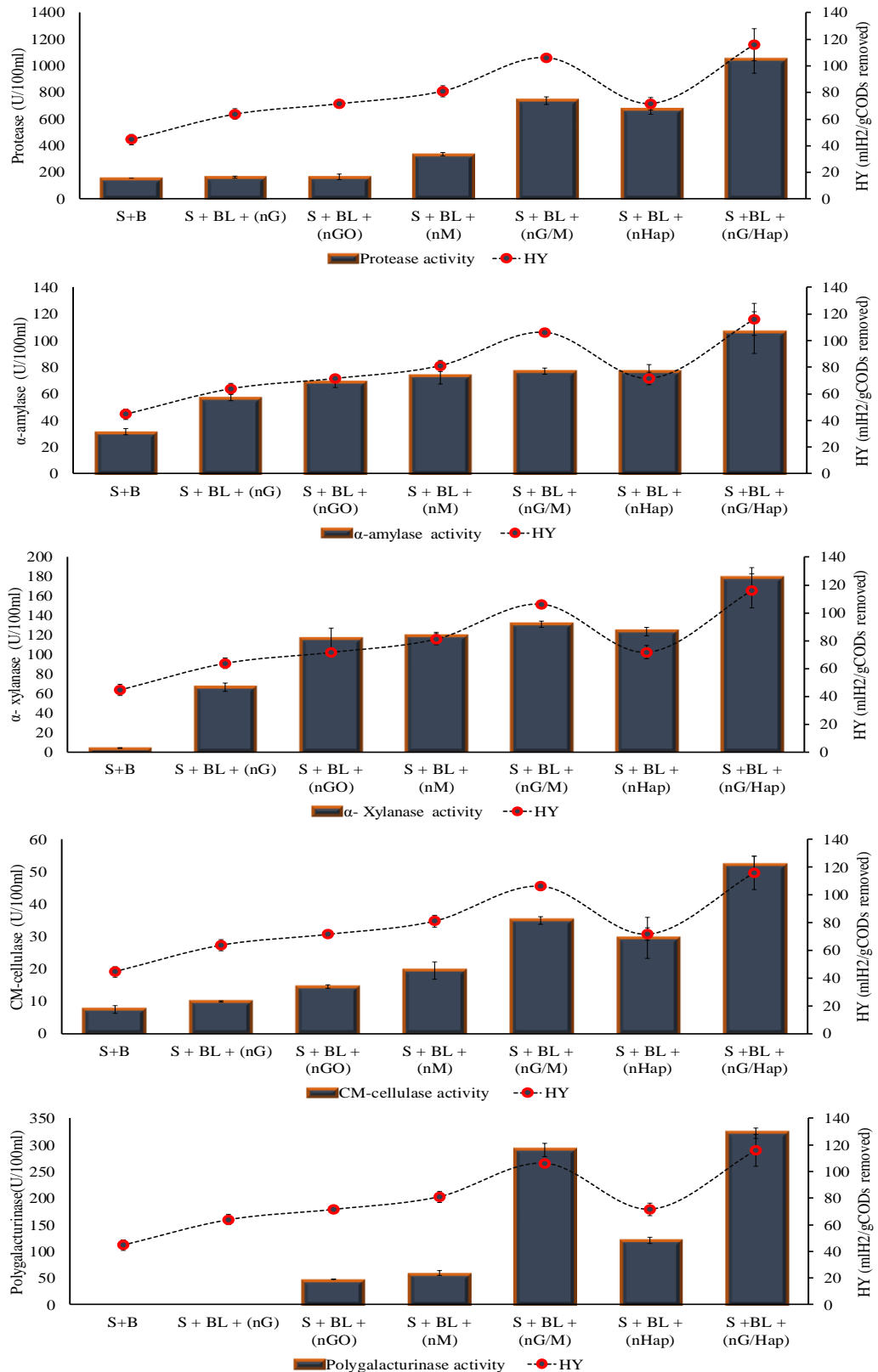
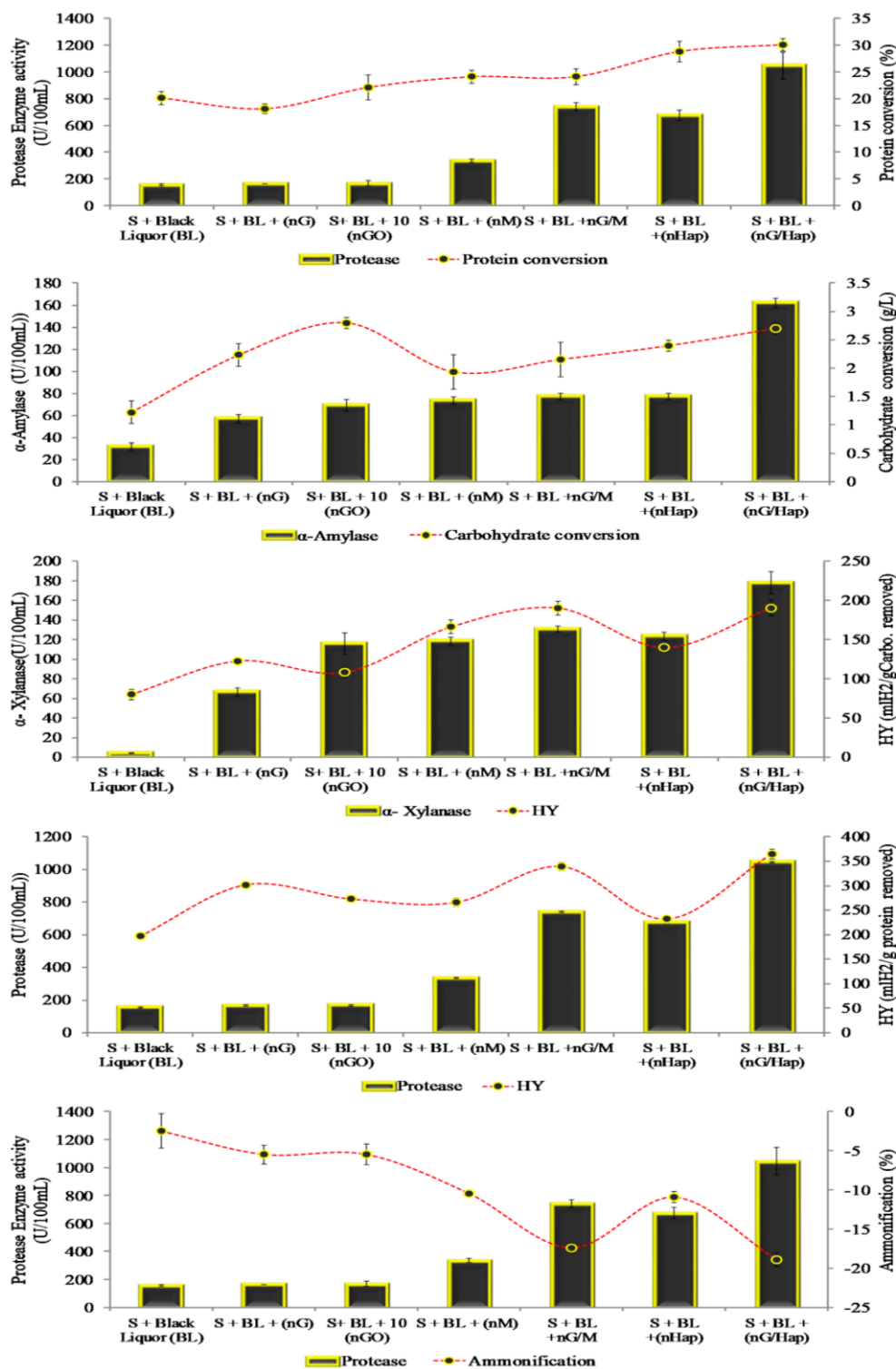


**Fig. 2d** enzymatic activities for anaerobes with free and combined nanoparticles for degradation of black liquor (BL)



**Figs. 3a** enzymatic activities and hydrogen yield (HY) for solely and dual nano-particles



**Figs. 3b** conversion of proteins, carbohydrates, CODs, ammonification process and hydrogen yield (HY) for anaerobes supplemented with solely and dual nano-particles

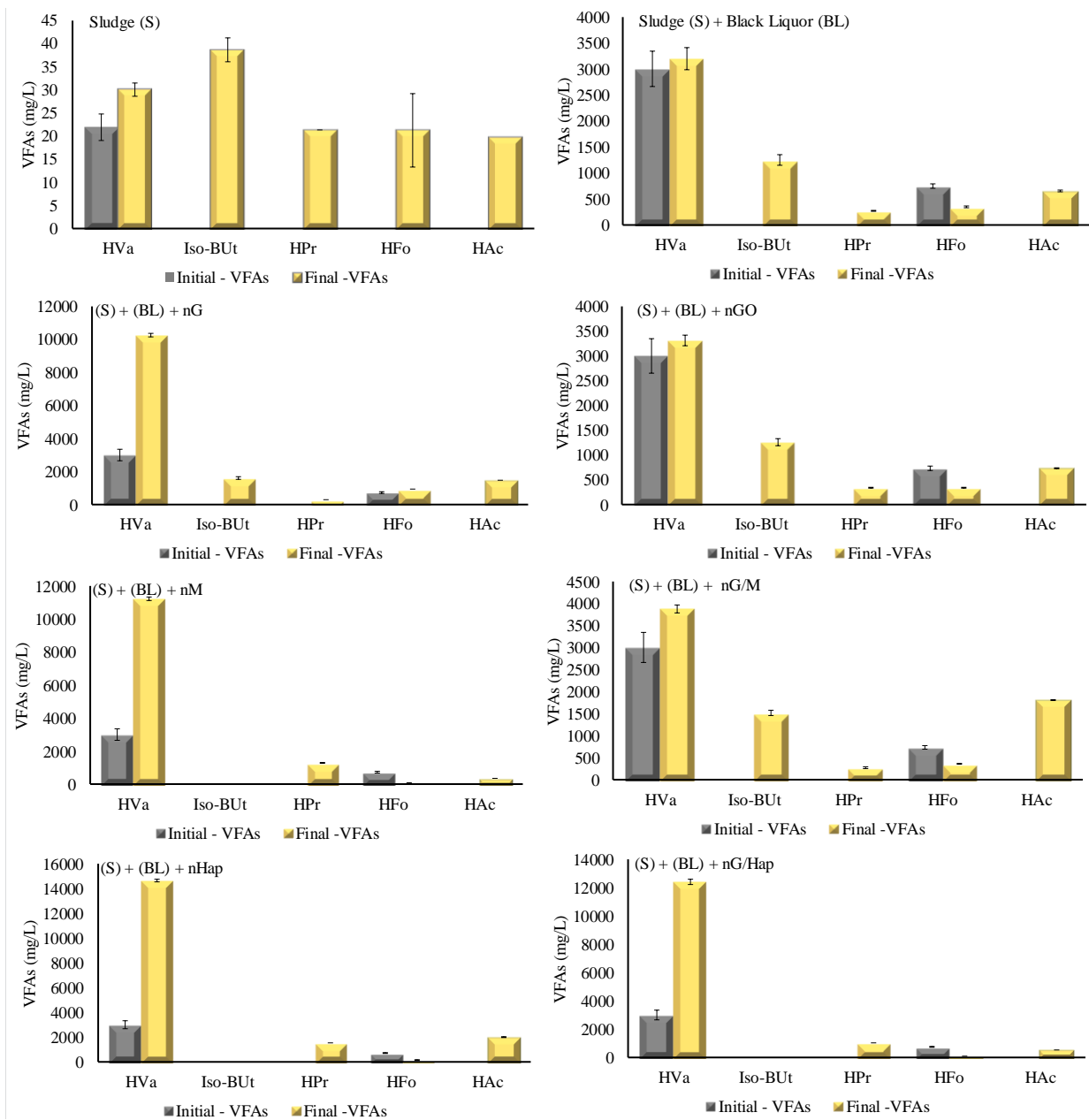


**Fig. 3c** metabolite by-products of the anaerobes producing hydrogen supplemented with solely and dual nano- particles from black liquor

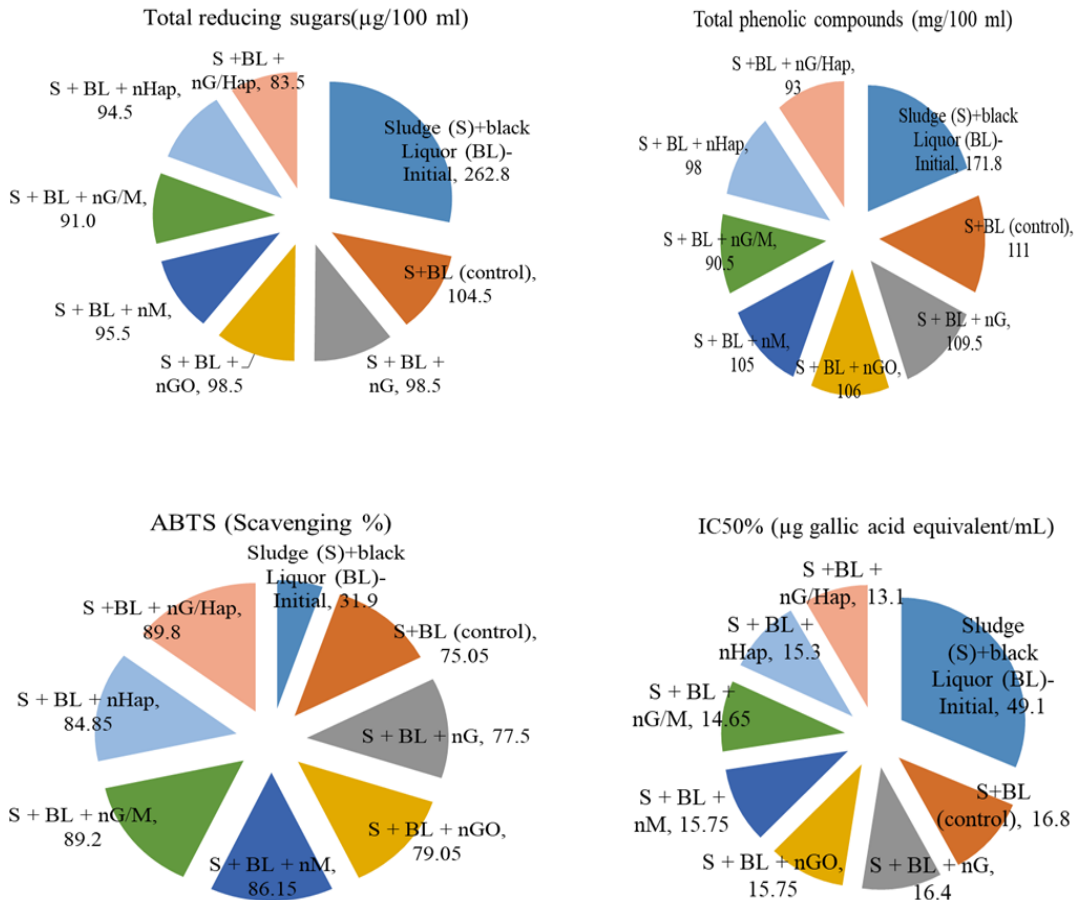


**Fig. 3d** total reducing sugars, total phenolic compounds, antioxidant activities –ABTS and the half maximal inhibitory concentration ( $\text{IC}_{50}$ ) of anaerobes with free and combined nanoparticles for degradation of black liquor

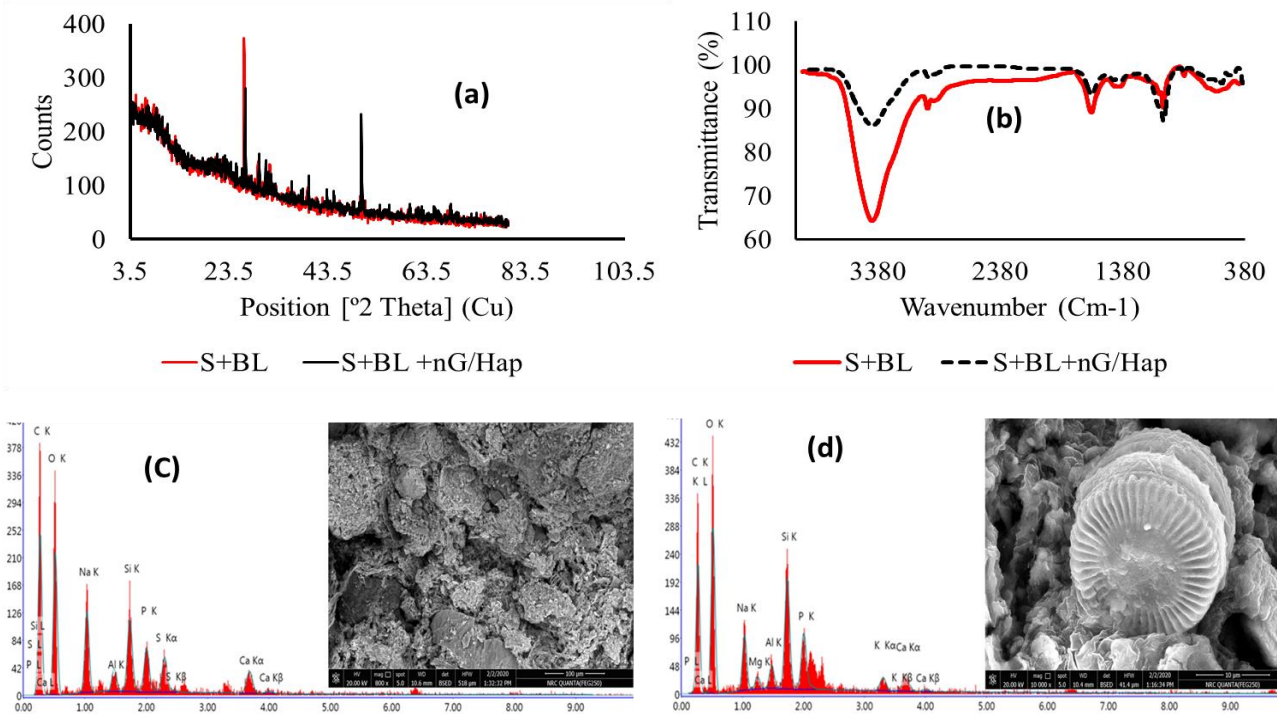


**Fig.4** X-Ray Diffraction (XRD) (a), Fourier-transform infrared spectroscopy (FTIR) (b), Scanning electron microscopy (SEM), and Energy dispersive X-ray (EDX), (c and d) for control samples (S+BL) and (S+B+nG/Hap) after fermentation

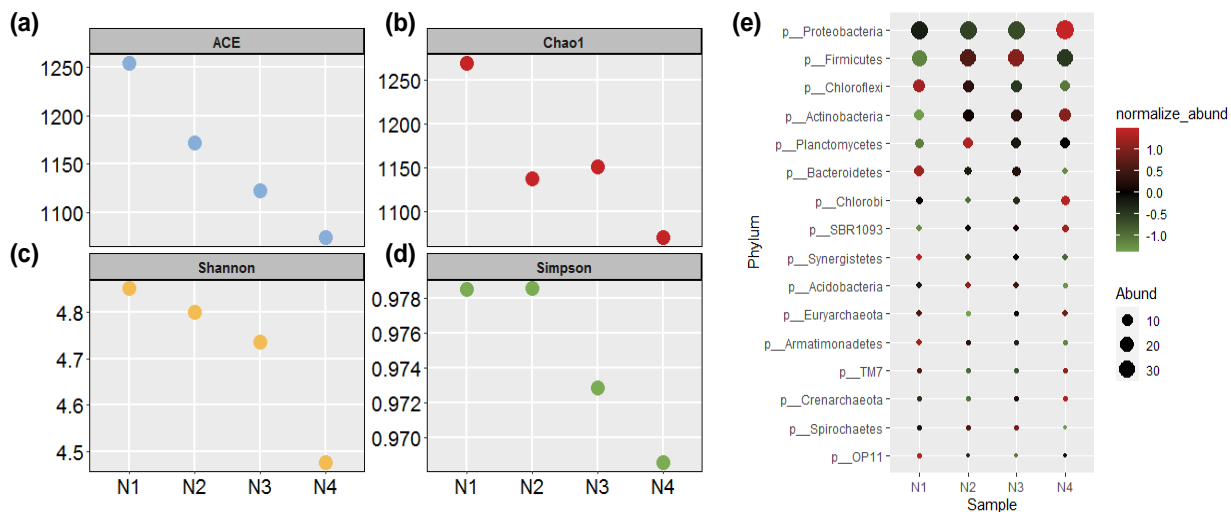


**Fig 5** Alpha-diversity and community structure of sludge supplemented with nG/Hap, nG/M, nM and nHap (N1, N2, N3 and N4). The ACE (a) and Chao1(b) indices are related to the absolute number of species in a given culture, while Simpson (c) and Shannon (d) indices are related to the distribution of species abundance of microbial communities. The major phyla (>0.1%) of the anaerobes (e) in the anaerobes immobilized on nanoparticles (N1,N2, N3 and N4). The size of the circle is proportional to the relative abundances of phyla in the digester. The color scale indicates the normalized relative abundances of phyla.

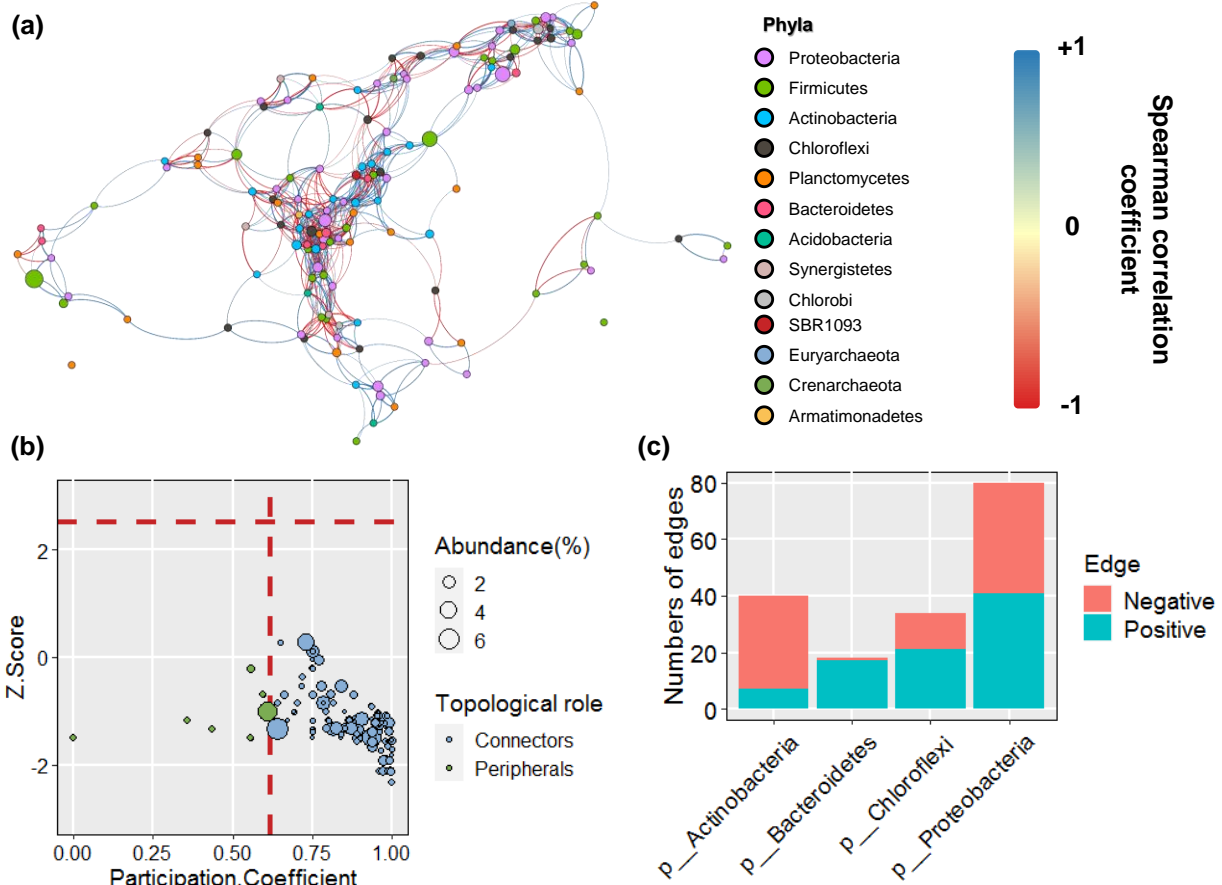


**Fig. 6** community ecology of the anaerobes (a) Phyla network uncovered the co-occurrence and co-exclusion between OTUs. Only the major OTUs (average abundance > 0.1%) and statistically significant correlations ( $P$ -value  $p<0.05$ ) are shown, resulting in the network consisted of 139 nodes and 774 edges. The size of the node is proportional to the RA of phylum in the digester and the node color represents the affiliated phylum of the node. Red and blue edges represent the co-exclusion and co-occurrence respectively. The wider edge gives an indication for the stronger correlations. (b) ZP-plot showing distribution of OTUs based on their module-based topological roles. The size of the circle is proportional to the average RA of phylum in the samples. (c) Numbers of positive and negative edges between the OTUs affiliated with *Firmicutes* and other major phyla.

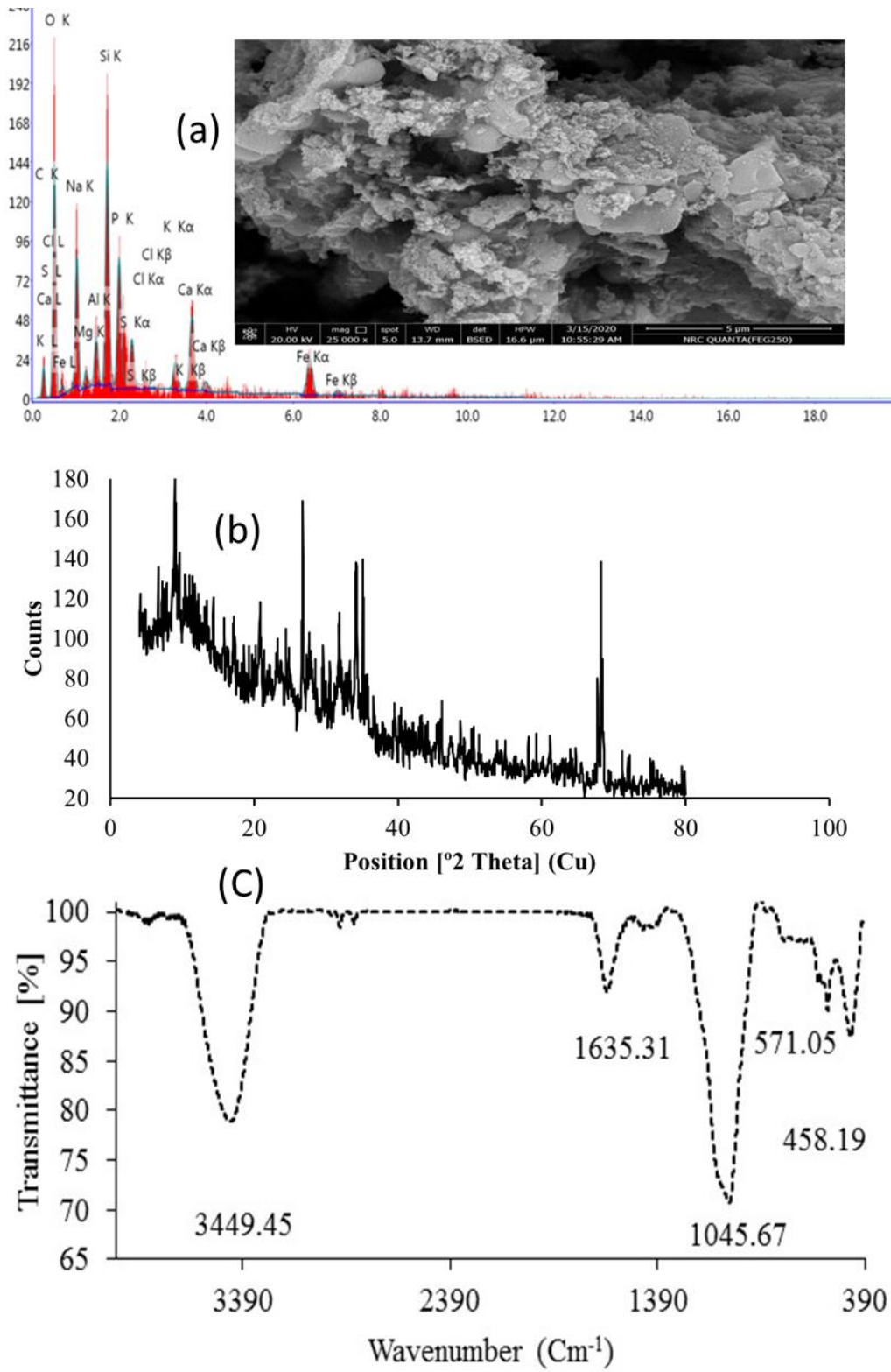


**Fig.7** scanning electron microscopy (SEM), Energy dispersive X-ray (EDX) (a), infrared absorption spectroscopy (FTIR) (b) and diffractometry of X-rays (XRD) (c) of the bio-char



Click here to access/download  
**Supplementary Material**  
Supplementary files.docx

**Declaration of Interest Statement**

This is to certify that there is no conflict of interest concerning this research

**On behalf of authors**

**Ahmed Tawfik**